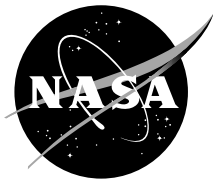


NASA/TM—2000–209891, Vol. 187



**Technical Report Series on the  
Boreal Ecosystem-Atmosphere Study (BOREAS)**

*Forrest G. Hall and Andrea Papagno, Editors*

**Volume 187**

**BOREAS TE-23 Canopy Architecture  
and Spectral Data from Hemispherical  
Photographs**

*P.M. Rich*

National Aeronautics and  
Space Administration

**Goddard Space Flight Center**  
Greenbelt, Maryland 20771

---

October 2000

## The NASA STI Program Office ... in Profile

Since its founding, NASA has been dedicated to the advancement of aeronautics and space science. The NASA Scientific and Technical Information (STI) Program Office plays a key part in helping NASA maintain this important role.

The NASA STI Program Office is operated by Langley Research Center, the lead center for NASA's scientific and technical information. The NASA STI Program Office provides access to the NASA STI Database, the largest collection of aeronautical and space science STI in the world. The Program Office is also NASA's institutional mechanism for disseminating the results of its research and development activities. These results are published by NASA in the NASA STI Report Series, which includes the following report types:

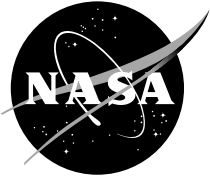
- **TECHNICAL PUBLICATION.** Reports of completed research or a major significant phase of research that present the results of NASA programs and include extensive data or theoretical analysis. Includes compilations of significant scientific and technical data and information deemed to be of continuing reference value. NASA's counterpart of peer-reviewed formal professional papers but has less stringent limitations on manuscript length and extent of graphic presentations.
- **TECHNICAL MEMORANDUM.** Scientific and technical findings that are preliminary or of specialized interest, e.g., quick release reports, working papers, and bibliographies that contain minimal annotation. Does not contain extensive analysis.
- **CONTRACTOR REPORT.** Scientific and technical findings by NASA-sponsored contractors and grantees.
- **CONFERENCE PUBLICATION.** Collected papers from scientific and technical conferences, symposia, seminars, or other meetings sponsored or cosponsored by NASA.
- **SPECIAL PUBLICATION.** Scientific, technical, or historical information from NASA programs, projects, and mission, often concerned with subjects having substantial public interest.
- **TECHNICAL TRANSLATION.** English-language translations of foreign scientific and technical material pertinent to NASA's mission.

Specialized services that complement the STI Program Office's diverse offerings include creating custom thesauri, building customized databases, organizing and publishing research results . . . even providing videos.

For more information about the NASA STI Program Office, see the following:

- Access the NASA STI Program Home Page at <http://www.sti.nasa.gov/STI-homepage.html>
- E-mail your question via the Internet to [help@sti.nasa.gov](mailto:help@sti.nasa.gov)
- Fax your question to the NASA Access Help Desk at (301) 621-0134
- Telephone the NASA Access Help Desk at (301) 621-0390
- Write to:  
NASA Access Help Desk  
NASA Center for Aerospace Information  
7121 Standard Drive  
Hanover, MD 21076-1320

NASA/TM—2000–209891, Vol. 187



**Technical Report Series on the  
Boreal Ecosystem-Atmosphere Study (BOREAS)**

*Forrest G. Hall and Andrea Papagno, Editors*

**Volume 187**

**BOREAS TE-23 Canopy Architecture  
and Spectral Data from Hemispherical  
Photographs**

*Paul M. Rich  
University of Kansas, Lawrence*

National Aeronautics and  
Space Administration

**Goddard Space Flight Center**  
Greenbelt, Maryland 20771

---

October 2000

Available from:

NASA Center for AeroSpace Information  
7121 Standard Drive  
Hanover, MD 21076-1320  
Price Code: A17

National Technical Information Service  
5285 Port Royal Road  
Springfield, VA 22161  
Price Code: A10

# **BOREAS TE-23 Canopy Architecture and Spectral Data from Hemispherical Photographs**

Paul M. Rich

## **Summary**

The BOREAS TE-23 team collected hemispherical photographs in support of its efforts to characterize and interpret information on estimates of canopy architecture and radiative transfer properties for most BOREAS study sites. Various OA, OBS, OJP, YJP, and YA sites in the boreal forest were measured from May to August 1994. The hemispherical photographs were used to derive values of LAI, leaf angle, gap fraction, and clumping index. This documentation describes these derived values. The derived data are stored in tabular ASCII files. The hemispherical photographs are stored in the original set of 42 CD-ROMs that were supplied by TE-23.

## **Table of Contents**

- 1) Data Set Overview
- 2) Investigator(s)
- 3) Theory of Measurements
- 4) Equipment
- 5) Data Acquisition Methods
- 6) Observations
- 7) Data Description
- 8) Data Organization
- 9) Data Manipulations
- 10) Errors
- 11) Notes
- 12) Application of the Data Set
- 13) Future Modifications and Plans
- 14) Software
- 15) Data Access
- 16) Output Products and Availability
- 17) References
- 18) Glossary of Terms
- 19) List of Acronyms
- 20) Document Information

## **1. Data Set Overview**

### **1.1 Data Set Identification**

BOREAS TE-23 Canopy Architecture and Spectral Data from Hemispherical Photographs

### **1.2 Data Set Introduction**

This canopy architecture and spectral data set provides BOREal Ecosystem-Atmosphere Study (BOREAS) investigators with extensive estimates of canopy architecture and radiative transfer properties for most BOREAS study sites in the Northern Study Area (NSA) and Southern Study Area (SSA).

### 1.3 Objectives/Purpose

The purpose of the work was to provide hemispherical photographs, taken in arrays looking upward from beneath the canopy, which are used to:

- Measure the angular distribution of gap fraction (proportion canopy opening).
- Estimate indices of canopy architecture, in particular leaf area index (LAI).
- Calculate indices of radiative transfer, in particular fraction of intercepted photosynthetically active radiation (FIPAR).

### 1.4 Summary of Parameters

Catalog of hemispherical photography: study area, site, date, roll identification, photograph identification, photograph location, photograph height, image archive information, and photograph quality.

Canopy architecture indices: effective LAI, foliage clump index, LAI, extinction coefficients, leaf angle distribution, mean tilt angle, mean tip angle error, skyview factor, gap fraction as a function of zenith angle.

Radiative transfer indices: direct FIPAR at monthly intervals, diffuse FIPAR.

### 1.5 Discussion

Hemispherical (fisheye) canopy photography is a technique for characterizing plant canopies using photographs taken looking upward through an extreme wide-angle lens (Evans and Coombe, 1959; Anderson, 1964; Percy, 1989; Rich, 1990). Typically, the viewing angle approaches or equals 180 degrees. The resulting photographs serve as permanent records of the geometry of canopy openings. The geometric distribution of openings can be measured precisely and used to estimate potential solar radiation blocked by the canopy and to estimate aspects of canopy architecture such as LAI and leaf angle distribution. Hemispherical photography has been used successfully in a broad range of studies involving microsite characterization and estimation of the fraction of photosynthetically active radiation (PAR) transmitted through canopy openings (e.g., Turton, 1988; Canham et al., 1990; Turner, 1990; Weiss et al., 1991; Mitchell and Whitmore, 1993; Rich et al., 1993). Hemispherical photographs can also supply gap fraction data for inversion models that calculate LAI and leaf inclination (Norman and Campbell, 1989; Chen and Black, 1992) and have been used successfully in various field studies (Bonhomme et al., 1974; Chen et al., 1991; Neumann and Shaw, 1989). Photographs can be taken along transects or in horizontal or vertical grid patterns to sample spatial heterogeneity within canopies (Galo et al., 1992; Lerda et al., 1992; Lin et al., 1992; Clark et al., 1996). Dynamics and temporal variation can be monitored by repeated sampling from the same camera positions (Rich et al., 1993).

The hemispherical photography data set is part of a hierarchical sampling approach for characterization of canopy architecture (Fournier et al., 1995, 1996). This approach involves a series of three sets of scale-tailored measurements, spanning from leaf to stand levels: 1) tree vectorization (Landry et al., 1997), involving detailed sampling of the three-dimensional distribution of canopy elements and crown form; 2) site characterization, involving detailed measurements of individual tree location, crown geometry, and understory cover; and 3) measurement of canopy geometry as seen from beneath -- involving acquisition of a multitemporal catalog of hemispherical photographs (this data set). This text focuses on description of the catalog of hemispherical photographs. The hemispherical photographs are stored in the original set of 42 Compact Disks - Read-Only Memory (CD-ROMs) that the BOREAS Information System (BORIS) received from Terrestrial Ecology (TE)-23 and submitted to the Oak Ridge National Laboratory (ORNL). Contact ORNL for further information regarding the hemispherical photography CD-ROMs.

## **1.6 Related Data Sets**

BOREAS RSS-04 1994 Southern Study Area Jack Pine LAI and FPAR Data  
BOREAS RSS-07 LAI, Gap Fraction, and fPAR Data  
BOREAS RSS-07 Regional LAI and FPAR Images From Ten-Day AVHRR-LAC Composites  
BOREAS RSS-07 Landsat TM Maps of LAI and Fpar  
BOREAS RSS-19 1994 CASI At-sensor Radiance and Reflectance Images  
BOREAS RSS-19 1996 CASI At-sensor Radiance and Reflectance Images  
BOREAS RSS-19 1994 Seasonal Understory Reflectance Data  
BOREAS TE-06 Multiband Vegetation Imager Data  
BOREAS TE-09 in situ Understory Spectral Reflectance within the NSA  
BOREAS TE-23 Map Plot Data

## **2. Investigator(s)**

### **2.1 Investigator(s) Name and Title**

Paul M. Rich Associate Professor  
University of Kansas

### **2.2 Title of Investigation**

Canopy Architecture of Boreal Forests: Using Hemispherical Photography for Study of Radiative Transport and Leaf Area Index

### **2.3 Contact Information**

#### **Contact 1:**

Dr. Paul M. Rich  
University of Kansas  
GIS and Environmental Modeling Laboratory (GEMLab)  
Nichols Hall, Space Technology Center  
2291 Irving Hill Drive  
Lawrence, KS 66045-2969 USA  
(913) 864-7769  
(913) 864-7789  
prich@oz.kbs.ukans.edu  
<http://www.gemlab.ukans.edu>

#### **Contact 2:**

Andrea Papagno  
Raytheon ITSS  
NASA GSFC  
Code 923  
Greenbelt, MD 20771  
(301) 286-3134  
(301) 286-0239 (fax)  
[Andrea.Papagno@gsfc.nasa.gov](mailto:Andrea.Papagno@gsfc.nasa.gov)

### 3. Theory of Measurements

The hemispherical lens was originally designed by Hill (1924) to provide a view of the entire sky for studies of cloud formation. Foresters and forest ecologists conceived of using photographic techniques to study the light environment under forest canopies by examining the pattern of sky obstruction. In particular, Evans and Coombe (1959) estimated sunlight penetration through forest canopy openings by overlaying diagrams of the sun track on hemispherical photographs. Later, Anderson (1964, 1971) provided a thorough theoretical treatment for calculating the penetration of direct and diffuse components of solar radiation through canopy openings as determined using hemispherical photographs. In recent years, many researchers have successfully used hemispherical canopy photography to study solar radiation penetration and canopy architecture (see reviews in Chazdon and Field, 1987; Rich, 1988, 1989, 1990; Becker et al., 1989), and to estimate LAI and other canopy indices (see Bonhomme et al., 1974; Chen et al., 1991; Neumann and Shaw, 1989). Detailed treatments of field and analytical methodology have been provided by Percy (1989) and Rich (1989, 1990).

Hemispherical photographs can be analyzed by hand using sampling grids (Anderson, 1964); however, hand analysis is extremely tedious and generally impractical for large numbers of photographs. Digital image analysis techniques have recently been developed that facilitate efficient analysis of large numbers of photographs (Chazdon and Field, 1987; Rich, 1988, 1989; Becker et al., 1989). Algorithms developed by Rich (1988, 1989) allow for rapid and flexible calculations. New technologies, such as charge-cooled device (CCD) cameras and inexpensive commercial digitization and storage on CD-ROM (Kodak PhotoCD), promise to permit still more efficient analysis and archiving of hemispherical imagery. A program, HemiView, became available in the prerelease form in 1998 for analysis of hemispherical imagery in standard graphics formats, including Kodak PhotoCD format. The full release of HemiView is expected during the summer of 1999 by Delta-T Devices, Ltd.

LAI is calculated following the methods of Norman and Campbell (1989), as modified by Chen and Black (1992). For theory of calculating LAI and other canopy indices, see the LAICalc manual (Rich et al., 1995), data documentation for Remote Sensing Science (RSS)-07 (Jing Chen), and the LAI intercomparison paper (Chen et al., 1997). LAICalc (including the manual) is available via anonymous ftp to oz.kbs.ukans.edu (in directory pub/laicalc) or from Paul Rich.

### 4. Equipment

#### 4.1 Sensor/Instrument Description

See Section 4.1.5.

#### 4.1.1 Collection Environment

Measurements were made in ambient environmental conditions from May to August 1994.

#### 4.1.2 Source/Platform

A self-leveling mount on a Bogen professional monopod was used to support the camera.

#### 4.1.3 Source/Platform Mission Objectives

Hemispherical photography was taken to aid in the calculation of radiative transport and LAI.

#### 4.1.4 Key Variables

Catalog of hemispherical photography: study area, site, date, roll identification, photograph identification, photograph location, photograph height, image archive information, and photograph quality.

Canopy architecture indices: effective LAI, foliage clump index, LAI, extinction coefficients, leaf angle distribution, mean tilt angle, mean tip angle error, skyview factor, gap fraction as a function of zenith angle.

Radiative transfer indices: direct FIPAR at monthly intervals, diffuse FIPAR.



#### **4.1.5 Principles of Operation**

Hemispherical photographs were taken with Kodak TMAX 400 ASA film pushed to 800 ASA, using a Nikkor 8-mm fisheye lens fitted on a Nikon FM2 body, and suspended pointing directly upward in a self-leveling mount on a Bogen professional monopod. A Nikon MF16 databack was used to imprint unique numbers on the edge of each photograph.

Video digitization and image processing were accomplished using:

- A Cohu high-resolution black-and-white CCD video camera for input.
- A Nikkor 55-mm micro lens with C-mount adapter for optics to the CCD video camera.
- An Imaging Technology PCVISIONplus framegrabber/display adapter for digitization (512 x 480 x 1 byte images).
- A Bencher Copymate II stand to support the video camera.
- A Marron Carrol positioner compound on a custom stand to position the negatives.
- An Aristo V56 lamp to backlight negatives.
- A Sony PVM1342Q analog RGB monitor to view images while processing.
- A 486 computer with a large-capacity hard drive as the computer platform.
- The hemispherical photograph analysis software CANOPY (Rich, 1989, 1990).

#### **4.1.6 Sensor/Instrument Measurement Geometry**

Hemispherical photographs were taken in arrays looking upward from beneath the canopy.

#### **4.1.7 Manufacturer of Sensor/Instrument**

Aristo V56 lamp  
Aristo Grid Lamp Products, Inc.  
35 Lumber Road  
Roslyn, NY 11576  
(516) 484-6141  
(516) 484-6992 (fax)

Bencher Copymate II stand  
831 N. Central Avenue  
Wood Dale, IL 60191  
(630) 238-1183  
(630) 238-1186 (fax)

Bogen professional monopod  
Bogen Photo Corp.  
565 East Crescent Ave.  
Ramsey, NJ 07446-0506 USA  
(201) 818-9500  
(201) 818-9177 (fax)  
info@bogenphoto.co

CANOPY (Rich 1989, 1990)

Cohu high-resolution black-and-white CCD video camera  
Cohu, Inc., Electronics Division  
5755 Kearny Villa Road  
San Diego, CA 92123, USA  
(619) 277-6700  
(619) 277-0221 (fax)

Hemispherical photograph analysis software  
Imaging Technology PCVISION plus framegrabber/display adapter  
Imaging Technology Incorporated  
55 Middlesex Turnpike  
Bedford, MA 01730  
(781) 275-2700  
(781) 275-9590 (fax)  
info@imaging.com

Nikkor 8-mm fisheye lens  
Nikkor 55-mm micro lens  
Nikon FM2 body  
Nikon MF16 databack  
Nikon, Inc.  
1300 Walt Whitman Rd.  
Melville, NY 11747-3064  
(516) 5474200

Sony PVM1342Q analog RGB monitor  
Sony Electronics, Inc.  
<http://www.sony.com/>

## **4.2 Calibration**

### **4.2.1 Specifications**

Hemispherical photography does not require calibration per se. An intercomparison of LAI estimates from hemispherical photography and other methods, in particular the LI-COR LAI-2000 (LI-COR, 1995), is provided by Chen et al. (1997). We found excellent agreement between LAI estimates obtained with the LI-COR LAI-2000 and analysis of hemispherical photographs (Chen et al., 1997; Rich et al., 1995; Rich, 1990 and 1989).

#### **4.2.1.1 Tolerance**

None given.

#### **4.2.2 Frequency of Calibration**

None given.

#### **4.2.3 Other Calibration Information**

To ensure consistency of hemispherical photograph image processing, a single trained technician was used for all photograph analyses. By performing repeated analyses on a subset of photographs from each of the major stand types, we were able to effectively quantify the "error" associated with photographic analysis (see Tables 1a, b, and c below).

Table 1. Summaries of LAI, diffuse FIPAR, and direct yearly FIPAR values for repeated analyses (i.e., independent analyses of the same photographs - trials) of hemispherical photographs at Old Black Spruce (OBS), Old Jack Pine (OJP), Young Jack Pine (YJP), and Old Aspen (OA) tower sites located in the BOREAS NSA and SSA. Means represent overall site means, which incorporate variability among trials and among photographs taken at the same site. Photographs were taken at horizontally and vertically spaced locations within each site. Standard deviations of trials reflect variability among repeated analyses. Standard deviations of photographs reflect the horizontal and vertical variability in LAI, diffuse FIPAR, and direct FIPAR for a particular site.

a) LAI

Site	Date	n_trials	n_photos	MEAN	STD_trials	STD_photos
NSA-OBS	12-Jul-1994	2	21	2.028	0.107	0.382
NSA-OJP	13-Jul-1994	2	19	1.320	0.182	0.246
NSA-YJP	17-Jul-1994	2	17	0.839	0.063	0.527
SSA-OA1	02-May-1994	3	30	1.237	0.324	0.621
SSA-OA2	14-May-1994	3	29	2.877	0.592	1.072
SSA-OA3	22-May-1994	3	25	1.899	0.488	0.448
SSA-OA4	02-Jun-1994	3	31	3.249	0.441	1.846
SSA-OA5	02-Jul-1994	3	31	3.044	0.380	0.875
SSA-OA6	04-Aug-1994	3	28	2.366	0.155	0.908
SSA-OBS	30-Jul-1994	3	30	1.670	0.124	0.782
SSA-OJP	29-Jul-1994	3	30	1.732	0.080	0.357
SSA-YJP	20-Jul-1994	2	24	0.835	0.054	0.717

b) Diffuse FIPAR

Site	Date	n_trials	n_photos	MEAN	STD_trials	STD_photos
NSA-OBS	12-Jul-1994	2	21	0.7540	0.0175	0.0900
NSA-OJP	13-Jul-1994	2	19	0.6163	0.0429	0.0892
NSA-YJP	17-Jul-1994	2	17	0.4611	0.0185	0.2530
SSA-OA1	02-May-1994	3	30	0.5818	0.1028	0.1364
SSA-OA2	14-May-1994	3	29	0.7740	0.0660	0.0719
SSA-OA3	22-May-1994	3	25	0.7385	0.0840	0.0878
SSA-OA4	02-Jun-1994	3	31	0.8384	0.0378	0.0697
SSA-OA5	02-Jul-1994	3	31	0.8371	0.0319	0.0654
SSA-OA6	04-Aug-1994	3	28	0.8173	0.0198	0.0618
SSA-OBS	30-Jul-1994	3	30	0.6883	0.0197	0.1805
SSA-OJP	29-Jul-1994	3	30	0.7161	0.0151	0.0794
SSA-YJP	20-Jul-1994	2	24	0.4494	0.0126	0.3011

c) Direct Yearly FIPAR

Site	Date	n_trials	n_photos	MEAN	STD_trials	STD_photos
NSA-OBS	12-Jul-1994	2	21	0.8113	0.0186	0.0640
NSA-OJP	13-Jul-1994	2	19	0.6827	0.0441	0.1010
NSA-YJP	17-Jul-1994	2	17	0.5380	0.0199	0.2660
SSA-OA1	02-May-1994	3	30	0.6193	0.0870	0.1622
SSA-OA2	14-May-1994	3	29	0.8388	0.0638	0.0882
SSA-OA3	22-May-1994	3	25	0.8169	0.0733	0.1459
SSA-OA4	02-Jun-1994	3	31	0.8851	0.0345	0.0725
SSA-OA5	02-Jul-1994	3	31	0.8957	0.0277	0.0689
SSA-OA6	04-Aug-1994	3	28	0.8525	0.0200	0.0748
SSA-OBS	30-Jul-1994	3	30	0.7914	0.0184	0.2082
SSA-OJP	29-Jul-1994	3	30	0.7575	0.0159	0.1079
SSA-YJP	20-Jul-1994	2	24	0.4310	0.0173	0.3649

## 5. Data Acquisition Methods

Hemispherical photographs were acquired in sample arrays at heights of 0.8, 1.5, and 2.5 m for each of the forested BOREAS tower flux sites and auxiliary sites. For the forested tower flux sites and other sites for which mapped plots were set up, hemispherical photographs were acquired during Intensive Field Campaign (IFC)-1 and IFC-2 at 10-m intervals along the central X axis of the mapped plot (5-m intervals for NSA-YJP). Typically, this corresponds to six sample locations for each tower flux site. The following table summarizes the location of these sampling arrays:

Site	Location
SSA-OBS	150 to 230 m (SE)
SSA-OJP	130 to 180 m (SE)
SSA-YJP	30 to 80 m (SE)
SSA-OA	70 to 120 m (SW)
NSA-OBS	80 to 130 m (SE)
NSA-OJP	70 to 120 m (SE)
NSA-YJP	120 to 150 m (SE)

Location refers to distance from the flux tower along the optical transect "B" line set up by Jing Chen, except in the case of SSA-OBS, where a "D" line is used (i.e., along the Y=20 line of the grid). For photographs taken in the mapped plots, the distance from the tower is given as the x-coordinate and the distance from the center line as the y-coordinate (except for SSA-OBS where the x-coordinate of the first mapped location is 0 for consistency with the TE-20/TE-22 mapped plot). SE or SW refers to the direction from the tower.

For the SSA-OA tower site, hemispherical photographs were acquired at intervals of 2-4 weeks throughout the growing season to enable analysis of phenological changes in the canopy.

For the auxiliary sites, hemispherical photographs were taken in a criss-cross array, at 10-m intervals along two 40-m-long transects placed at right angles and crossing in the middle. A sample location was centered at one of the focal sample locations used for biometry sampling, and additional sample locations were spaced at 10-m and 20-m intervals from the center location in each of the four cardinal directions (to the north, south, east, and west), for a total of nine sample locations. Dates of the auxiliary photographs range from during IFC-1 to during IFC-2.

Additional sets of hemispherical photographs were acquired 1) at sample locations with the mixed forest mapped plots (MIX1, MIX2, MIX3, and MIX4); 2) at locations with light sensors in SSA-OJP, SSA-OBS, NSA-OA, NSA-OJP, NSA-YJP, and NSA-OBS; and 3) along vertical transects at TE towers in SSA-M3, SSA-OJP, and SSA-OBS.

Hemispherical photograph negatives were video digitized at a resolution of 512 (h) x 480 (v) x 7 bits using the hemispherical photograph analysis system CANOPY (Rich, 1989, 1990). A full archive of these photographs will be provided to BORIS. All hemispherical photographs were also archived in Kodak PhotoCD format. Two sets of Kodak PhotoCDs were produced; one is available through Paul Rich's laboratory, and the other was provided to BORIS.

## 6. Observations

### 6.1 Data Notes

All pertinent data are contained in the data files. The hemispherical photographs are stored in the original set of 42 CD-ROMs that BORIS received from TE-23 and submitted to ORNL. Contact ORNL for further information regarding the hemispherical photography CD-ROMs.

### 6.2 Field Notes

Field notes were recorded in notebooks and are available from ORNL.

## 7. Data Description

### 7.1 Spatial Characteristics

The overall BOREAS project was conducted at a 1,000-km by 1,000-km regional area. The SSA was defined to cover a 130-km by 90-km area and the NSA was defined to cover a 40-km by 30-km area. Each tower flux site was at the scale of approximately 1 km by 1 km.

#### 7.1.1 Spatial Coverage

The SSA and NSA measurement sites and associated North American Datum of 1983 (NAD83) coordinates are:

NSA-9BS, site id T6R5S, Lat/Long: 55.90802°N, 98.51865°W  
UTM Zone 14, N: 6,195,947.0, E: 530,092.0.

NSA-9BS, site id S8W0S, Lat/Long: 55.76824°N, 97.84024°W  
UTM Zone 14, N: 6,180,894.9, E: 572,761.9.

NSA-9BS, site id T0W1S, Lat/Long: 55.78239°N, 97.80937°W  
UTM Zone 14, N: 6,182,502.0, E: 574,671.7.

NSA-9BS, site id T3U9S, Lat/Long: 55.83083°N, 97.98339°W  
UTM Zone 14, N: 6,187,719.2, E: 563,679.1.

NSA-9BS, site id T4U8S, Lat/Long: 55.83913°N, 97.99325°W  
UTM Zone 14, N: 6,188,633.4, E: 563,048.2.

NSA-9BS, site id T0P8S, Lat/Long: 55.88351°N, 98.80225°W  
UTM Zone 14, N: 6,193,132.0, E: 512,370.1.

NSA-9BS, site id T0P7S, Lat/Long: 55.88371°N, 98.82345°W  
UTM Zone 14, N: 6,193,151.1, E: 511,043.9.

NSA-9BS, site id U5W5S, Lat/Long: 55.9061°N, 97.70986°W  
UTM Zone 14, N: 6,196,380.8, E: 580,655.5.

NSA-9BS, site id U6W5S, Lat/Long: 55.91021°N, 97.70281°W  
UTM Zone 14, N: 6,196,846.5, E: 581,087.8.

NSA-9BS, site id T7R9S, Lat/Long: 55.91506°N, 98.44877°W  
UTM Zone 14, N: 6,196,763.6, E: 534,454.5.

NSA-9BS, site id T5Q7S, Lat/Long: 55.9161°N, 98.64022°W  
UTM Zone 14, N: 6,196,800.5, E: 522,487.2.

NSA-9BS, site id T8S4S, Lat/Long: 55.91689°N, 98.37111°W  
UTM Zone 14, N: 6,197,008.6, E: 539,306.4.

NSA-9JP, site id Q3V3P, Lat/Long: 55.55712°N, 98.02473°W  
UTM Zone 14, N: 6,157,222.2, E: 561,517.9.

NSA-9JP, site id 99O9P, Lat/Long: 55.88173°N, 99.03952°W  
UTM Zone 14, N: 6,192,917.5, E: 497,527.8.

NSA-9JP, site id T7S9P, Lat/Long: 55.89486°N, 98.30037°W  
UTM Zone 14, N: 6,194,599.1, E: 543,752.4.

NSA-9JP, site id T8S9P, Lat/Long: 55.90456°N, 98.28385°W  
UTM Zone 14, N: 6,195,688.9, E: 544,774.3.

NSA-9JP, site id T8Q9P, Lat/Long: 55.93219°N, 98.6105°W  
UTM Zone 14, N: 6,198,601.4, E: 524,334.5.

NSA-9JP, site id T9Q8P, Lat/Long: 55.93737°N, 98.59568°W  
UTM Zone 14, N: 6,199,183.2, E: 525,257.1.

NSA-9OA, site id T2Q6A, Lat/Long: 55.88691°N, 98.67479°W  
UTM Zone 14, N: 6,193,540.7, E: 520,342.0.

NSA-ASP, site id P7V1A, Lat/Long: 55.50253°N, 98.07478°W  
UTM Zone 14, N: 6,151,103.7, E: 558,442.1.

NSA-ASP, site id R8V8A, Lat/Long: 55.67779°N, 97.8926°W  
UTM Zone 14, N: 6,170,774.8, E: 569,638.4.

NSA-ASP, site id T4U5A, Lat/Long: 55.84757°N, 98.04329°W  
UTM Zone 14, N: 6,189,528.2, E: 559,901.6.

NSA-ASP, site id S9P3A, Lat/Long: 55.88576°N, 98.87621°W  
UTM Zone 14, N: 6,193,371.6, E: 507,743.3.

NSA-ASP, site id T8S4A, Lat/Long: 55.91856°N, 98.37041°W  
UTM Zone 14, N: 6,197,194.6, E: 539,348.3.

NSA-ASP, site id Q3V2A, Lat/Long: 55.56227°N, 98.02635°W  
UTM Zone 14, N: 6,157,793.5, E: 561,407.9.

NSA-ASP, site id V5X7A, Lat/Long: 55.97396°N, 97.48565°W  
UTM Zone 14, N: 6,204,216.6, E: 594,506.1.

NSA-ASP, site id W0Y5A, Lat/Long: 56.00339°N, 97.3355°W  
UTM Zone 14, N: 6,207,706.6, E: 603,796.6.

NSA-MIX, site id Q1V2M, Lat/Long: 55.54568°N, 98.03769°W  
UTM Zone 14, N: 6,155,937.3, E: 560,718.3.

NSA-MIX, site id T0P5M, Lat/Long: 55.88911°N, 98.85662°W  
UTM Zone 14, N: 6,193,747.3, E: 508,967.7.

NSA-OBS, site id T3R8T, Lat/Long: 55.88007°N, 98.48139°W  
UTM Zone 14, N: 6,192,853.4, E: 532,444.5.

NSA-OJP, site id T7Q8T, Lat/Long: 55.92842°N, 98.62396°W  
UTM Zone 14, N: 6,198,176.3, E: 523,496.2.

NSA-YJP, site id T8S9T, Lat/Long: 55.89575°N, 98.28706°W  
UTM Zone 14, N: 6,194,706.9, E: 544,583.9.

SSA-9BS, site id D0H6S, Lat/Long: 53.64877°N, 105.29534°W  
UTM Zone 13, N: 5,944,263.4, E: 480,508.7.

SSA-9BS, site id G2L7S, Lat/Long: 53.90349°N, 104.63785°W  
UTM Zone 13, N: 5,972,844.3, E: 523,793.6.

SSA-9BS, site id G2I4S, Lat/Long: 53.93021°N, 105.13964°W  
UTM Zone 13, N: 5,975,766.3, E: 490,831.4.

SSA-9BS, site id H2D1S, Lat/Long: 54.06199°N, 105.92545°W  
UTM Zone 13, N: 5,990,814.4, E: 439,428.1.

SSA-9BS, site id H1E4S, Lat/Long: 54.04093°N, 105.73581°W  
UTM Zone 13, N: 5,988,326.1, E: 451,815.7.

SSA-9BS, site id G6K8S, Lat/Long: 53.94446°N, 104.759°W  
UTM Zone 13, N: 5,977,146.9, E: 515,847.9.

SSA-9BS, site id G9I4S, Lat/Long: 53.99877°N, 105.11805°W  
UTM Zone 13, N: 5,983,169.1, E: 492,291.2.

SSA-9JP, site id F5I6P, Lat/Long: 53.86608°N, 105.11175°W  
UTM Zone 13, N: 5,968,627.1, E: 492,651.3.

SSA-9JP, site id F7J1P, Lat/Long: 53.88211°N, 105.03226°W  
UTM Zone 13, N: 5,970,405.6, E: 497,879.4.

SSA-9JP, site id F7J0P, Lat/Long: 53.88336°N, 105.05115°W  
UTM Zone 13, N: 5,970,323.3, E: 496,667.0.

SSA-9JP, site id G1K9P, Lat/Long: 53.9088°N, 104.74812°W  
UTM Zone 13, N: 5,973,404.5, E: 516,546.7.

SSA-9JP, site id G4K8P, Lat/Long: 53.91883°N, 104.76401°W  
UTM Zone 13, N: 5,974,516.6, E: 515,499.1.

SSA-9JP, site id G7K8P, Lat/Long: 53.95882°N, 104.77148°W  
UTM Zone 13, N: 5,978,963.8, E: 514,994.2.

SSA-9JP, site id G8L6P, Lat/Long: 53.96558°N, 104.63755°W  
UTM Zone 13, N: 5,979,752.7, E: 523,778.0.

SSA-9JP, site id I2I8P, Lat/Long: 54.11181°N, 105.05107°W  
UTM Zone 13, N: 5,995,963.1, E: 496,661.4.

SSA-9OA, site id C3B7T, Lat/Long: 53.62889°N, 106.19779°W  
UTM Zone 13, N: 5,942,899.9, E: 420,790.5.

SSA-ASP, site id B9B7A, Lat/Long: 53.59098°N, 106.18693°W  
UTM Zone 13, N: 5,938,447.2, E: 421,469.8.

SSA-ASP, site id E7C3A, Lat/Long: 53.84741°N, 106.08112°W  
UTM Zone 13, N: 5,966,863.1, E: 428,905.9.

SSA-ASP, site id D6L9A, Lat/Long: 53.66879°N, 104.6388°W  
UTM Zone 13, N: 5,946,733.2, E: 523,864.0.

SSA-ASP, site id D6H4A, Lat/Long: 53.70828°N, 105.31546°W  
UTM Zone 13, N: 5,951,112.1, E: 479,177.5.

SSA-ASP, site id D9G4A, Lat/Long: 53.74019°N, 105.46929°W  
UTM Zone 13, N: 5,954,718.4, E: 469,047.1.

SSA-MIX, site id D9I1M, Lat/Long: 53.7254°N, 105.20643°W  
UTM Zone 13, N: 5,952,989.7, E: 486,379.7.

SSA-MIX, site id H3D1M, Lat/Long: 54.066°N, 105.92982°W  
UTM Zone 13, N: 5,991,042.3, E: 439,178.4.

SSA-MIX, site id H2D1M, Lat/Long: 54.06535°N, 105.92706°W  
UTM Zone 13, N: 5,991,190.3, E: 439,327.7.

SSA-MIX, site id D9I1M, Lat/Long: 53.7254°N, 105.20643°W  
UTM Zone 13, N: 5,952,989.7, E: 486,379.7.

SSA-MIX, site id D9I1M, Lat/Long: 53.7254°N, 105.20643°W  
UTM Zone 13, N: 5,952,989.7, E: 486,379.7.

SSA-MIX, site id D9I1M, Lat/Long: 53.7254°N, 105.20643°W  
UTM Zone 13, N: 5,952,989.7, E: 486,379.7.

SSA-MIX, site id D9I1M, Lat/Long: 53.7254°N, 105.20643°W  
UTM Zone 13, N: 5,952,989.7, E: 486,379.7.

SSA-MIX, site id D9I1M, Lat/Long: 53.7254°N, 105.20643°W  
UTM Zone 13, N: 5,952,989.7, E: 486,379.7.

SSA-MIX, site id F1N0M, Lat/Long: 53.80594°N, 104.533°W  
UTM Zone 13, N: 5,962,031.8, E: 530,753.7.

SSA-MIX, site id G4I3M, Lat/Long: 53.9375°N, 105.14246°W  
UTM Zone 13, N: 5,976,354.9, E: 490,677.3.

SSA-OBS, site id G8I4T, Lat/Long: 53.98717°N, 105.11779°W  
UTM Zone 13, N: 5,982,100.5, E: 492,276.5.

SSA-OJP, site id G2L3T, Lat/Long: 53.91634°N, 104.69203°W  
UTM Zone 13, N: 5,974,257.5, E: 520,227.7.

SSA-YJP, site id F8L6T, Lat/Long: 53.87581°N, 104.64529°W  
UTM Zone 13, N: 5,969,762.5, E: 523,320.2.

### 7.1.2 Spatial Coverage Map

Not available.

### 7.1.3 Spatial Resolution

The photographs were acquired at 10-m intervals (5-m intervals in NSA-YJP), along a transect that was a) typically 50 m long at the tower flux sites, and b) two 40-m-long transects placed at right angles and crossing in the middle for the auxiliary flux sites. In terms of remote sensing, this gives good estimates for a pixel size of 30 m x 30 m or finer.

### 7.1.4 Projection

Not applicable.

### 7.1.5 Grid Description

For tower sites, the location of the grid was determined based on distance and direction from a known reference location (typically the Tower Flux (TF) or TE tower). The following is a summary of the grid layout:

Site	Location	Width	Grid Interval
SSA-OBS	150 to 30 m (SE)*	+/- 20 m	10 m
SSA-OJP	130 to 180 m (SE)	+/- 30 m	10 m
SSA-YJP	30 to 80 m (SE)	+/- 30 m	10 m
SSA-OA	70 to 120 m (SW)	+/- 20 m	10 m
NSA-OBS	80 to 130 m (SE)	+/- 30 m	10 m
NSA-OJP	70 to 120 m (SE)	+/- 30 m	10 m
NSA-YJP	120 to 150 m (SE)	+/- 20 m	5 m

Location refers to distance from the flux tower along the optical (Jing Chen's RSS-07) transect "B" line. All transect lines are clearly marked by pink flags, and the sample locations within the mapped plots are marked with stakes (orange wooden stakes in most sites, blue PVC tubes at SSA-OBS). The mapped plot coordinates are marked on the stakes, with the distance from the tower as the x-coordinate, and the distance from the centerline as the y-coordinate (except for SSA-OBS where the x-coordinate of the first mapped location is 0 for consistency with the TE-20/TE-22 mapped plot). SE or SW refers to the direction from the tower. Width refers to dimensions of the mapped plot on either side of the optical transect "B" line, except in the case of SSA-OBS, where a "D" line is used, i.e., along the Y=20 line of the grid. Grid interval refers to spacing of grid stakes.

## 7.2 Temporal Characteristics

### 7.2.1 Temporal Coverage

All measurements pertain to the summer of 1994:

- Hemispherical photographs were taken for IFC-1 and IFC-2 at the tower flux sites.
- A phenological series was taken at the SSA-OA and mixed sites between early May and September.
- Auxiliary sites were photographed between June and August.

### 7.2.2 Temporal Coverage Map

Not available.

### 7.2.3 Temporal Resolution

The hemispherical photography indices should generally apply to all of the summer of 1994 for conifer sites. This was verified by comparing calculated indices for the tower flux sites between IFC-1 and IFC-2. For the SSA-OA and mixed sites, we were able to observe phenological changes from May through September.

## 7.3 Data Characteristics

### 7.3.1 Parameter/Variable

The parameters contained in the data files on the CD-ROM are

#### CANOPY\_ARCH\_INV

Column Name

```

-----
SITE_NAME
SUB_SITE
DATE_OBS
TE23_FILM_ROLL_ID
BEGIN_PRINT_NUM
END_PRINT_NUM
CD1_ID
CD2_ID

```



BEGIN\_CD1\_IMAGE\_NUM  
END\_CD1\_IMAGE\_NUM  
PHOTO\_QUALITY  
ANALYSIS\_STATUS  
COMMENTS  
CRTFCN\_CODE  
REVISION\_DATE

**CANOPY\_ARCH\_DAT**

Column Name

-----  
SITE\_NAME  
SUB\_SITE  
DATE\_OBS  
TE23\_FILM\_ROLL\_ID  
TE23\_PHOTO\_ID  
TE\_X\_GRID  
TE\_Y\_GRID  
PHOTO\_LOCATION  
MEAN\_PHOTO\_HT\_AGL  
LEAF\_AREA\_INDX\_EFFEC  
EXTINCT\_COEF\_0\_TO\_15  
EXTINCT\_COEF\_15\_TO\_30  
EXTINCT\_COEF\_30\_TO\_45  
EXTINCT\_COEF\_45\_TO\_60  
EXTINCT\_COEF\_60\_TO\_75  
LEAF\_AREA\_0\_TO\_15  
LEAF\_AREA\_15\_TO\_30  
LEAF\_AREA\_30\_TO\_45  
LEAF\_AREA\_45\_TO\_60  
LEAF\_AREA\_60\_TO\_75  
MEAN\_TIP\_ANG  
STD\_ERR\_TIP\_ANG  
SKYVIEW\_FACTOR  
CLUMP\_FACTOR  
LEAF\_AREA\_INDX  
INDIR\_SITE\_FACT\_NOCOS  
INDIR\_SITE\_FACT\_COS  
DIR\_SITE\_FACT\_NOCOS  
DIR\_SITE\_FACT\_COS  
FIPAR\_DIF  
FIPAR\_DIR\_YEAR  
FIPAR\_JUN  
FIPAR\_JUL\_OR\_MAY  
FIPAR\_AUG\_OR\_APR  
FIPAR\_SEP\_OR\_MAR  
FIPAR\_OCT\_OR\_FEB  
FIPAR\_NOV\_OR\_JAN  
FIPAR\_DEC  
TE23\_IMAGE\_ID  
THRESHOLD  
CD1\_ID  
CD1\_IMAGE\_NUM  
CD2\_ID

CD2\_IMAGE\_NUM  
GAP\_FRACT\_0\_TO\_5  
GAP\_FRACT\_5\_TO\_10  
GAP\_FRACT\_10\_TO\_15  
GAP\_FRACT\_15\_TO\_20  
GAP\_FRACT\_20\_TO\_25  
GAP\_FRACT\_25\_TO\_30  
GAP\_FRACT\_30\_TO\_35  
GAP\_FRACT\_35\_TO\_40  
GAP\_FRACT\_40\_TO\_45  
GAP\_FRACT\_45\_TO\_50  
GAP\_FRACT\_50\_TO\_55  
GAP\_FRACT\_55\_TO\_60  
GAP\_FRACT\_60\_TO\_65  
GAP\_FRACT\_65\_TO\_70  
GAP\_FRACT\_70\_TO\_75  
CRTFCN\_CODE  
REVISION\_DATE

**CANOPY\_ARCH\_AV**

Column Name

-----  
SITE\_NAME  
SUB\_SITE  
DATE\_OBS  
SRC\_FILE  
MEAN\_PHOTO\_HT\_AGL  
NUM\_PHOTOS  
MEAN\_LEAF\_AREA\_INDX  
SDEV\_LEAF\_AREA\_INDX  
MEAN\_LEAF\_AREA\_INDX\_EFFEC  
SDEV\_LEAF\_AREA\_INDX\_EFFEC  
MEAN\_EXTINCT\_COEF\_0\_TO\_15  
SDEV\_EXTINCT\_COEF\_0\_TO\_15  
MEAN\_EXTINCT\_COEF\_15\_TO\_30  
SDEV\_EXTINCT\_COEF\_15\_TO\_30  
MEAN\_EXTINCT\_COEF\_30\_TO\_45  
SDEV\_EXTINCT\_COEF\_30\_TO\_45  
MEAN\_EXTINCT\_COEF\_45\_TO\_60  
SDEV\_EXTINCT\_COEF\_45\_TO\_60  
MEAN\_EXTINCT\_COEF\_60\_TO\_75  
SDEV\_EXTINCT\_COEF\_60\_TO\_75  
MEAN\_LEAF\_AREA\_0\_TO\_15  
SDEV\_LEAF\_AREA\_0\_TO\_15  
MEAN\_LEAF\_AREA\_15\_TO\_30  
SDEV\_LEAF\_AREA\_15\_TO\_30  
MEAN\_LEAF\_AREA\_30\_TO\_45  
SDEV\_LEAF\_AREA\_30\_TO\_45  
MEAN\_LEAF\_AREA\_45\_TO\_60  
SDEV\_LEAF\_AREA\_45\_TO\_60  
MEAN\_LEAF\_AREA\_60\_TO\_75  
SDEV\_LEAF\_AREA\_60\_TO\_75  
MEAN\_MEAN\_TIP\_ANG  
SDEV\_MEAN\_TIP\_ANG

MEAN\_STD\_ERR\_TIP\_ANG  
SDEV\_STD\_ERR\_TIP\_ANG  
MEAN\_SKYVIEW\_FACTOR  
SDEV\_SKYVIEW\_FACTOR  
MEAN\_INDIR\_SITE\_FACT\_NOCOS  
SDEV\_INDIR\_SITE\_FACT\_NOCOS  
MEAN\_INDIR\_SITE\_FACT\_COS  
SDEV\_INDIR\_SITE\_FACT\_COS  
MEAN\_DIR\_SITE\_FACT\_NOCOS  
SDEV\_DIR\_SITE\_FACT\_NOCOS  
MEAN\_DIR\_SITE\_FACT\_COS  
SDEV\_DIR\_SITE\_FACT\_COS  
MEAN\_FIPAR\_DIF  
SDEV\_FIPAR\_DIF  
MEAN\_FIPAR\_DIR\_YEAR  
SDEV\_FIPAR\_DIR\_YEAR  
MEAN\_FIPAR\_JUN  
SDEV\_FIPAR\_JUN  
MEAN\_FIPAR\_JUL\_OR\_MAY  
SDEV\_FIPAR\_JUL\_OR\_MAY  
MEAN\_FIPAR\_AUG\_OR\_APR  
SDEV\_FIPAR\_AUG\_OR\_APR  
MEAN\_FIPAR\_SEP\_OR\_MAR  
SDEV\_FIPAR\_SEP\_OR\_MAR  
MEAN\_FIPAR\_OCT\_OR\_FEB  
SDEV\_FIPAR\_OCT\_OR\_FEB  
MEAN\_FIPAR\_NOV\_OR\_JAN  
SDEV\_FIPAR\_NOV\_OR\_JAN  
MEAN\_FIPAR\_DEC  
SDEV\_FIPAR\_DEC  
MEAN\_GAP\_FRACT\_0\_TO\_5  
SDEV\_GAP\_FRACT\_0\_TO\_5  
MEAN\_GAP\_FRACT\_5\_TO\_10  
SDEV\_GAP\_FRACT\_5\_TO\_10  
MEAN\_GAP\_FRACT\_10\_TO\_15  
SDEV\_GAP\_FRACT\_10\_TO\_15  
MEAN\_GAP\_FRACT\_15\_TO\_20  
SDEV\_GAP\_FRACT\_15\_TO\_20  
MEAN\_GAP\_FRACT\_20\_TO\_25  
SDEV\_GAP\_FRACT\_20\_TO\_25  
MEAN\_GAP\_FRACT\_25\_TO\_30  
SDEV\_GAP\_FRACT\_25\_TO\_30  
MEAN\_GAP\_FRACT\_30\_TO\_35  
SDEV\_GAP\_FRACT\_30\_TO\_35  
MEAN\_GAP\_FRACT\_35\_TO\_40  
SDEV\_GAP\_FRACT\_35\_TO\_40  
MEAN\_GAP\_FRACT\_40\_TO\_45  
SDEV\_GAP\_FRACT\_40\_TO\_45  
MEAN\_GAP\_FRACT\_45\_TO\_50  
SDEV\_GAP\_FRACT\_45\_TO\_50  
MEAN\_GAP\_FRACT\_50\_TO\_55  
SDEV\_GAP\_FRACT\_50\_TO\_55  
MEAN\_GAP\_FRACT\_55\_TO\_60  
SDEV\_GAP\_FRACT\_55\_TO\_60

MEAN\_GAP\_FRACT\_60\_TO\_65  
 SDEV\_GAP\_FRACT\_60\_TO\_65  
 MEAN\_GAP\_FRACT\_65\_TO\_70  
 SDEV\_GAP\_FRACT\_65\_TO\_70  
 MEAN\_GAP\_FRACT\_70\_TO\_75  
 SDEV\_GAP\_FRACT\_70\_TO\_75  
 CRTFCN\_CODE  
 REVISION\_DATE

### 7.3.2 Variable Description/Definition

The descriptions of the parameters contained in the data files on the CD-ROM are:

#### CANOPY\_ARCH\_INV

Column Name	Description
SITE_NAME	The identifier assigned to the site by BOREAS, in the format SSS-TTT-CCCCC, where SSS identifies the portion of the study area: NSA, SSA, REG, TRN, and TTT identifies the cover type for the site, 999 if unknown, and CCCCC is the identifier for site, exactly what it means will vary with site type.
SUB_SITE	The identifier assigned to the sub-site by BOREAS, in the format GGGGG-IIIII, where GGGGG is the group associated with the sub-site instrument, e.g. HYD06 or STAFF, and IIIII is the identifier for sub-site, often this will refer to an instrument.
DATE_OBS	The date on which the data were collected.
TE23_FILM_ROLL_ID	The TE-23 roll identification-- the first letter specifies one of three cameras: "s", "n", or "j" -- the numeric characters specify the roll number for the particular camera setup.
BEGIN_PRINT_NUM	The particular print number which begins the photos for that site.
END_PRINT_NUM	The particular print number which ends the photos for that site.
CD1_ID	Identification Code for PhotoCD, copy one.
CD2_ID	Identification Code for PhotoCD, copy two.
BEGIN_CD1_IMAGE_NUM	The particular image number which begins the photos for that site.
END_CD1_IMAGE_NUM	The particular image number which ends the photos for that site.
PHOTO_QUALITY	The TE-23 provided or assessed quality of the photograph(s).
ANALYSIS_STATUS	Tells whether the analysis of the photo by TE-23 is fully complete or not.
COMMENTS	Descriptive information to clarify or enhance the understanding of the other entered data.
CRTFCN_CODE	The BOREAS certification level of the data. Examples are CPI (Checked by PI), CGR (Certified by Group), PRE (Preliminary), and CPI-??? (CPI but questionable).
REVISION_DATE	The most recent date when the information in the referenced data base table record was revised.

**CANOPY\_ARCH\_DATA**

Column Name	Description
SITE_NAME	The identifier assigned to the site by BOREAS, in the format SSS-TTT-CCCCC, where SSS identifies the portion of the study area: NSA, SSA, REG, TRN, and TTT identifies the cover type for the site, 999 if unknown, and CCCCC is the identifier for site, exactly what it means will vary with site type.
SUB_SITE	The identifier assigned to the sub-site by BOREAS, in the format GGGGG-IIIII, where GGGGG is the group associated with the sub-site instrument, e.g. HYD06 or STAFF, and IIIII is the identifier for sub-site, often this will refer to an instrument.
DATE_OBS	The date on which the data were collected.
TE23_FILM_ROLL_ID	The TE-23 roll identification-- the first letter specifies one of three cameras: "s", "n", or "j" -- the numeric characters specify the roll number for the particular camera setup.
TE23_PHOTO_ID	The TE-23 photograph identification number corresponding to a particular camera setup. Photograph identification numbers are imprinted on the negative with a databack.
TE_X_GRID	The X-grid coordinate where the photograph was acquired. For tower sites, with the exception of SSA-OBS, the X-grid coordinate corresponds to the distance from the tower.
TE_Y_GRID	The Y-grid coordinate where the photograph was acquired. For tower sites, with the exception of SSA_OBS, Y=0 corresponds with J. Chen's "B" line for optical measurements. For the SSA_OBS, Y=0 corresponds with J. Chen's "D" line f.
PHOTO_LOCATION	The location where the hemispherical photograph was acquired.
MEAN_PHOTO_HT_AGL	The mean height above ground level where the group of hemispherical photographs were taken.
LEAF_AREA_INDX_EFFEC	Effective leaf area index, based on hemispherical photograph analysis. Note effective LAI must be corrected by a clumping factor to calculate LAI (Chen et al. 1995).
EXTINCT_COEF_0_TO_15	Extinction coefficient calculated from hemispherical photographs for zenith angle centered at 7.5 degrees, with a range from 0 to 15 degrees.
EXTINCT_COEF_15_TO_30	Extinction coefficient calculated from hemispherical photographs for zenith angle centered at 22.5 degrees, with a range from 15 to 30 degrees.
EXTINCT_COEF_30_TO_45	Extinction coefficient calculated from hemispherical photographs for zenith angle centered at 37.5 degrees, with a range from 30 to 45 degrees.
EXTINCT_COEF_45_TO_60	Extinction coefficient calculated from

	hemispherical photographs for zenith angle centered at 52.5 degrees, with a range from 45 to 60 degrees.
EXTINCT_COEF_60_TO_75	Extinction coefficient calculated from hemispherical photographs for zenith angle centered at 67.5 degrees, with a range from 60 to 75 degrees.
LEAF_AREA_0_TO_15	Leaf area for zenith angle centered at 7.5 degrees, with a range from 0 to 15 degrees.
LEAF_AREA_15_TO_30	Leaf area for zenith angle centered at 22.5 degrees, with a range from 15 to 30 degrees.
LEAF_AREA_30_TO_45	Leaf area for zenith angle centered at 37.5 degrees, with a range from 30 to 45 degrees.
LEAF_AREA_45_TO_60	Leaf area for zenith angle centered at 52.5 degrees, with a range from 45 to 60 degrees.
LEAF_AREA_60_TO_75	Leaf area for zenith angle centered at 67.5 degrees, with a range from 60 to 75 degrees.
MEAN_TIP_ANG	The mean tip angle of the leaves observed.
STD_ERR_TIP_ANG	The standard error of the mean leaf tip angle.
SKYVIEW_FACTOR	The proportion of unobscured sky, weighted appropriately to account for angle of incidence on a horizontal plane.
CLUMP_FACTOR	Clumping factor, by which effective LAI is divided to calculate LAI.
LEAF_AREA_INDX	Leaf area index, based on hemispherical photograph analysis, including the clumping factor correction (Chen et al. 1995).
INDIR_SITE_FACT_NOCOS	Indirect (diffuse) site factor without cosine correction for horizontal plane-- equivalent to angular openness.
INDIR_SITE_FACT_COS	Indirect (diffuse) site factor with cosine correction for horizontal plane-- equivalent to skyview factor.
DIR_SITE_FACT_NOCOS	Direct site factor without cosine correction for horizontal plane.
DIR_SITE_FACT_COS	Direct site factor with cosine correction for horizontal plane.
FIPAR_DIF	Fraction of intercepted diffuse PAR calculated assuming an isotropic distribution of diffuse illuminance (equivalent to $1 - \text{INDIR\_SITE\_FACT\_COS}$ )
FIPAR_DIR_YEAR	The fraction of intercepted direct PAR calculated assuming an isotropic distribution of diffuse illuminance for the year.
FIPAR_JUN	Daily fraction of intercepted direct PAR from hemispheric photos assuming sun angles in June.
FIPAR_JUL_OR_MAY	Daily fraction of intercepted direct PAR from hemispheric photos assuming sun angles in July or May.
FIPAR_AUG_OR_APR	Daily fraction of intercepted direct PAR from hemispheric photos assuming sun angles in August or April.
FIPAR_SEP_OR_MAR	Daily fraction of intercepted direct PAR from hemispheric photos assuming sun angles in September or March.

FIPAR_OCT_OR_FEB	Daily fraction of intercepted direct PAR from hemispheric photos assuming sun angles in October or February.
FIPAR_NOV_OR_JAN	Daily fraction of intercepted direct PAR from hemispheric photos assuming sun angles in November or January.
FIPAR_DEC	Daily fraction of intercepted direct PAR from hemispheric photos assuming sun angles in December
TE23_IMAGE_ID	File name of image file (CANOPY program format) used for analysis of hemispherical photograph.
THRESHOLD	Threshold used in CANOPY program for density slice classification of image into obscured and open sky directions.
CD1_ID	Identification Code for PhotoCD, copy one.
CD1_IMAGE_NUM	Photo number on PhotoCD, copy one.
CD2_ID	Identification Code for PhotoCD, copy two.
CD2_IMAGE_NUM	Photo number on PhotoCD, copy two.
GAP_FRACT_0_TO_5	Gap fraction for zenith angle centered at 2.5 degrees, with a range from 0 to 5 degrees.
GAP_FRACT_5_TO_10	Gap fraction for zenith angle centered at 7.5 degrees, with a range from 5 to 10 degrees.
GAP_FRACT_10_TO_15	Gap fraction for zenith angle centered at 12.5 degrees, with a range from 10 to 15 degrees.
GAP_FRACT_15_TO_20	Gap fraction for zenith angle centered at 17.5 degrees, with a range from 15 to 20 degrees.
GAP_FRACT_20_TO_25	Gap fraction for zenith angle centered at 22.5 degrees, with a range from 20 to 25 degrees.
GAP_FRACT_25_TO_30	Gap fraction for zenith angle centered at 27.5 degrees, with a range from 25 to 30 degrees.
GAP_FRACT_30_TO_35	Gap fraction for zenith angle centered at 32.5 degrees, with a range from 30 to 35 degrees.
GAP_FRACT_35_TO_40	Gap fraction for zenith angle centered at 37.5 degrees, with a range from 35 to 40 degrees.
GAP_FRACT_40_TO_45	Gap fraction for zenith angle centered at 42.5 degrees, with a range from 40 to 45 degrees.
GAP_FRACT_45_TO_50	Gap fraction for zenith angle centered at 47.5 degrees, with a range from 45 to 50 degrees.
GAP_FRACT_50_TO_55	Gap fraction for zenith angle centered at 52.5 degrees, with a range from 50 to 55 degrees.
GAP_FRACT_55_TO_60	Gap fraction for zenith angle centered at 57.5 degrees, with a range from 55 to 60 degrees.
GAP_FRACT_60_TO_65	Gap fraction for zenith angle centered at 62.5 degrees, with a range from 60 to 65 degrees.
GAP_FRACT_65_TO_70	Gap fraction for zenith angle centered at 67.5 degrees with a range from 65 to 70 degrees.
GAP_FRACT_70_TO_75	Gap fraction for zenith angle centered at 72.5 degrees, with a range from 70 to 75 degrees.
CRTFCN_CODE	The BOREAS certification level of the data. Examples are CPI (Checked by PI), CGR (Certified by Group), PRE (Preliminary), and CPI-??? (CPI but questionable).
REVISION_DATE	The most recent date when the information in the referenced data base table record was revised.

**CANOPY\_ARCH\_AVG**

Column Name	Description
SITE_NAME	The identifier assigned to the site by BOREAS, in the format SSS-TTT-CCCCC, where SSS identifies the portion of the study area: NSA, SSA, REG, TRN, and TTT identifies the cover type for the site, 999 if unknown, and CCCCC is the identifier for site, exactly what it means will vary with site type.
SUB_SITE	The identifier assigned to the sub-site by BOREAS, in the format GGGGG-IIIII, where GGGGG is the group associated with the sub-site instrument, e.g. HYD06 or STAFF, and IIIII is the identifier for sub-site, often this will refer to an instrument.
DATE_OBS	The date on which the data were collected.
SRC_FILE	The file containing the hemispherical data used to calculate the averages and standard deviations.
MEAN_PHOTO_HT_AGL	The mean height above ground level where the group of hemispherical photographs were taken.
NUM_PHOTOS	The number of hemispherical photos used to derive the given statistical values.
MEAN_LEAF_AREA_INDX	The average of the leaf area index, based on hemispherical photograph analysis, including the clumping factor correction (Chen et al. 1995).
SDEV_LEAF_AREA_INDX	The standard deviation of the leaf area index, based on hemispherical photograph analysis, including the clumping factor correction (Chen et al. 1995).
MEAN_LEAF_AREA_INDX_EFFEC	The average of the effective leaf area index, based on hemispherical photograph analysis. Note effective LAI must be corrected by a clumping factor to calculate LAI (Chen et al. 1995).
SDEV_LEAF_AREA_INDX_EFFEC	The standard deviation of the effective leaf area index, based on hemispherical photograph analysis. Note effective LAI must be corrected by a clumping factor to calculate LAI (Chen et al. 1995).
MEAN_EXTINCT_COEF_0_TO_15	The average of the extinction coefficient from hemispherical photographs for zenith angle centered at 7.5 degrees, with a range from 0 to 15 degrees.
SDEV_EXTINCT_COEF_0_TO_15	The standard deviation of the extinction coefficient from hemispherical photographs for zenith angle centered at 7.5 degrees, with a range from 0 to 15 degrees.
MEAN_EXTINCT_COEF_15_TO_30	The average of the extinction coefficient from hemispherical photographs for zenith angle centered at 22.5 degrees, with a range from 15 to 30 degrees.
SDEV_EXTINCT_COEF_15_TO_30	The standard deviation of the extinction coefficient from hemispherical photographs for



MEAN_EXTINCT_COEF_30_TO_45	zenith angle centered at 22.5 degrees, with a range from 15 to 30 degrees.
SDEV_EXTINCT_COEF_30_TO_45	The average of the extinction coefficient from hemispherical photographs for zenith angle centered at 37.5 degrees, with a range from 30 to 45 degrees.
MEAN_EXTINCT_COEF_45_TO_60	The standard deviation of the extinction coefficient from hemispherical photographs for zenith angle centered at 37.5 degrees, with a range from 30 to 45 degrees.
SDEV_EXTINCT_COEF_45_TO_60	The average of the extinction coefficient from hemispherical photographs for zenith angle centered at 52.5 degrees, with a range from 45 to 60 degrees.
MEAN_EXTINCT_COEF_60_TO_75	The standard deviation of the extinction coefficient from hemispherical photographs for zenith angle centered at 52.5 degrees, with a range from 45 to 60 degrees.
SDEV_EXTINCT_COEF_60_TO_75	The average of the extinction coefficient from hemispherical photographs for zenith angle centered at 67.5 degrees, with a range from 60 to 75 degrees.
MEAN_LEAF_AREA_0_TO_15	The standard deviation of the extinction coefficient from hemispherical photographs for zenith angle centered at 67.5 degrees, with a range from 60 to 75 degrees.
SDEV_LEAF_AREA_0_TO_15	The average of leaf area for zenith angle centered at 7.5 degrees, with a range from 0 to 15 degrees.
MEAN_LEAF_AREA_15_TO_30	The standard deviation of leaf area for zenith angle centered at 7.5 degrees, with a range from 0 to 15 degrees.
SDEV_LEAF_AREA_15_TO_30	The average of leaf area for zenith angle centered at 22.5 degrees, with a range from 15 to 30 degrees.
MEAN_LEAF_AREA_30_TO_45	The standard deviation of leaf area for zenith angle centered at 22.5 degrees, with a range from 15 to 30 degrees.
SDEV_LEAF_AREA_30_TO_45	The average of leaf area for zenith angle centered at 37.5 degrees, with a range from 30 to 45 degrees.
MEAN_LEAF_AREA_45_TO_60	The standard deviation of leaf area for zenith angle centered at 37.5 degrees, with a range from 30 to 45 degrees.
SDEV_LEAF_AREA_45_TO_60	The average of leaf area for zenith angle centered at 52.5 degrees, with a range from 45 to 60 degrees.
MEAN_LEAF_AREA_60_TO_75	The standard deviation of leaf area for zenith angle centered at 52.5 degrees, with a range from 45 to 60 degrees.
SDEV_LEAF_AREA_60_TO_75	The average of leaf area for zenith angle centered at 67.5 degrees, with a range from 60 to 75 degrees.
	The standard deviation of leaf area for zenith

	angle centered at 67.5 degrees, with a range from 60 to 75 degrees.
MEAN_MEAN_TIP_ANG	The average of the mean leaf tip angles.
SDEV_MEAN_TIP_ANG	The standard deviation of the mean leaf tip angles.
MEAN_STD_ERR_TIP_ANG	The average of the standard error of the mean leaf tip angle.
SDEV_STD_ERR_TIP_ANG	The standard deviation of the standard error of the mean leaf tip angle.
MEAN_SKYVIEW_FACTOR	The average of the proportion of unobscured sky, weighted appropriately to account for the angle of incidence on a horizontal plane (Reifsnyder 1967).
SDEV_SKYVIEW_FACTOR	The standard deviation of the proportion of unobscured sky, weighted appropriately to account for the angle of incidence on a horizontal plane (Reifsnyder 1967).
MEAN_INDIR_SITE_FACT_NOCOS	The average of the indirect site factor without cosine correction for horizontal plane-- equivalent to angular openness.
SDEV_INDIR_SITE_FACT_NOCOS	The standard deviation of the indirect site factor without cosine correction for horizontal plane-- equivalent to angular openness.
MEAN_INDIR_SITE_FACT_COS	The average of the indirect site factor with cosine correction for horizontal plane-- equivalent to skyview factor.
SDEV_INDIR_SITE_FACT_COS	The standard deviation of the indirect site factor with cosine correction for horizontal plane-- equivalent to skyview factor.
MEAN_DIR_SITE_FACT_NOCOS	The average of the direct site factor without cosine correction for horizontal plane.
SDEV_DIR_SITE_FACT_NOCOS	The standard deviation of the direct site factor without cosine correction for horizontal plane.
MEAN_DIR_SITE_FACT_COS	The average of the direct site factor with cosine correction for horizontal plane.
SDEV_DIR_SITE_FACT_COS	The standard deviation of the direct site factor with cosine correction for horizontal plane.
MEAN_FIPAR_DIF	The average of the fraction of intercepted diffuse PAR calculated assuming an isotropic distribution of diffuse illuminance (equivalent to 1 - INDIR_SITE_FACT_COS).
SDEV_FIPAR_DIF	The standard deviation of the fraction of intercepted diffuse PAR calculated assuming an isotropic distribution of diffuse illuminance (equivalent to 1 - INDIR_SITE_FACT_COS).
MEAN_FIPAR_DIR_YEAR	The average of the fraction of intercepted direct PAR calculated assuming an isotropic distribution of diffuse illuminance for the year.
SDEV_FIPAR_DIR_YEAR	The standard deviation of the fraction of intercepted direct PAR calculated assuming an isotropic distribution of diffuse illuminance for the year.
MEAN_FIPAR_JUN	Average of the daily fraction of intercepted direct PAR for the hemispherical photos assuming

SDEV_FIPAR_JUN	sun angles in June. Standard deviation of the daily fraction of intercepted direct PAR for June.
MEAN_FIPAR_JUL_OR_MAY	Average of the daily fraction of intercepted direct PAR for the hemispherical photos assuming sun angles in July or May.
SDEV_FIPAR_JUL_OR_MAY	Standard deviation of the daily fraction of intercepted direct PAR for July or May.
MEAN_FIPAR_AUG_OR_APR	Average of the daily fraction of intercepted direct PAR for the hemispherical photos assuming sun angles in August or April.
SDEV_FIPAR_AUG_OR_APR	Standard deviation of the daily fraction of intercepted direct PAR for August or April.
MEAN_FIPAR_SEP_OR_MAR	Average of the daily fraction of intercepted direct PAR for the hemispherical photos assuming sun angles in September or May.
SDEV_FIPAR_SEP_OR_MAR	Standard deviation of the daily fraction of intercepted direct PAR for September or May.
MEAN_FIPAR_OCT_OR_FEB	Average of the daily fraction of intercepted direct PAR for the hemispherical photos assuming sun angles in October or February.
SDEV_FIPAR_OCT_OR_FEB	Standard deviation of the daily fraction of intercepted direct PAR for October or February.
MEAN_FIPAR_NOV_OR_JAN	Average of the daily fraction of intercepted direct PAR for the hemispherical photos assuming sun angles in November or January.
SDEV_FIPAR_NOV_OR_JAN	Standard deviation of the daily fraction of intercepted direct PAR for November or January.
MEAN_FIPAR_DEC	Average of the daily fraction of intercepted direct PAR for the hemispherical photos assuming sun angles in December.
SDEV_FIPAR_DEC	Standard deviation of the daily fraction of intercepted direct PAR for December.
MEAN_GAP_FRACT_0_TO_5	The average gap fraction for zenith angle centered at 2.5 degrees, with a range from 0 to 5 degrees.
SDEV_GAP_FRACT_0_TO_5	The standard deviation of the gap fraction for zenith angle centered at 2.5 degrees, with a range from 0 to 5 degrees.
MEAN_GAP_FRACT_5_TO_10	The average gap fraction for zenith angle centered at 7.5 degrees, with a range from 5 to 10 degrees.
SDEV_GAP_FRACT_5_TO_10	The standard deviation of the gap fraction for zenith angle centered at 7.5 degrees, with a range from 5 to 10 degrees.
MEAN_GAP_FRACT_10_TO_15	The average gap fraction for zenith angle centered at 12.5 degrees, with a range from 10 to 15 degrees.
SDEV_GAP_FRACT_10_TO_15	The standard deviation of the gap fraction for zenith angle centered at 12.5 degrees, with a range from 10 to 15 degrees.
MEAN_GAP_FRACT_15_TO_20	The average gap fraction for zenith angle centered at 17.5 degrees, with a range from 15 to 20 degrees.

SDEV_GAP_FRACT_15_TO_20	The standard deviation of the gap fraction for zenith angle centered at 17.5 degrees, with a range from 15 to 20 degrees.
MEAN_GAP_FRACT_20_TO_25	The average gap fraction for zenith angle centered at 22.5 degrees, with a range from 20 to 25 degrees.
SDEV_GAP_FRACT_20_TO_25	The standard deviation of the gap fraction for zenith angle centered at 22.5 degrees, with a range from 20 to 25 degrees.
MEAN_GAP_FRACT_25_TO_30	The average gap fraction for zenith angle centered at 27.5 degrees, with a range from 25 to 30 degrees.
SDEV_GAP_FRACT_25_TO_30	The standard deviation of the gap fraction for zenith angle centered at 27.5 degrees, with a range from 25 to 30 degrees.
MEAN_GAP_FRACT_30_TO_35	The average gap fraction for zenith angle centered at 32.5 degrees, with a range from 30 to 35 degrees.
SDEV_GAP_FRACT_30_TO_35	The standard deviation of the gap fraction for zenith angle centered at 32.5 degrees, with a range from 30 to 35 degrees.
MEAN_GAP_FRACT_35_TO_40	The average gap fraction for zenith angle centered at 37.5 degrees, with a range from 35 to 40 degrees.
SDEV_GAP_FRACT_35_TO_40	The standard deviation of the gap fraction for zenith angle centered at 37.5 degrees, with a range from 35 to 40 degrees.
MEAN_GAP_FRACT_40_TO_45	The average gap fraction for zenith angle centered at 42.5 degrees, with a range from 40 to 45 degrees.
SDEV_GAP_FRACT_40_TO_45	The standard deviation of the gap fraction for zenith angle centered at 42.5 degrees, with a range from 40 to 45 degrees.
MEAN_GAP_FRACT_45_TO_50	The average gap fraction for zenith angle centered at 47.5 degrees, with a range from 45 to 50 degrees.
SDEV_GAP_FRACT_45_TO_50	The standard deviation of the gap fraction for zenith angle centered at 47.5 degrees, with a range from 45 to 50 degrees.
MEAN_GAP_FRACT_50_TO_55	The average gap fraction for zenith angle centered at 52.5 degrees, with a range from 50 to 55 degrees.
SDEV_GAP_FRACT_50_TO_55	The standard deviation of the gap fraction for zenith angle centered at 52.5 degrees, with a range from 50 to 55 degrees.
MEAN_GAP_FRACT_55_TO_60	The average gap fraction for zenith angle centered at 57.5 degrees, with a range from 55 to 60 degrees.
SDEV_GAP_FRACT_55_TO_60	The standard deviation of the gap fraction for zenith angle centered at 57.5 degrees, with a range from 55 to 60 degrees.
MEAN_GAP_FRACT_60_TO_65	The average gap fraction for zenith angle centered at 62.5 degrees, with a range from 60 to 65 degrees.

SDEV_GAP_FRACT_60_TO_65	The standard deviation of the gap fraction for zenith angle centered at 62.5 degrees, with a range from 60 to 65 degrees.
MEAN_GAP_FRACT_65_TO_70	The average gap fraction for zenith angle centered at 67.5 degrees, with a range from 65 to 70 degrees.
SDEV_GAP_FRACT_65_TO_70	The standard deviation of the gap fraction for zenith angle centered at 67.5 degrees, with a range from 65 to 70 degrees.
MEAN_GAP_FRACT_70_TO_75	The average gap fraction for zenith angle centered at 72.5 degrees, with a range from 70 to 75 degrees.
SDEV_GAP_FRACT_70_TO_75	The standard deviation of the gap fraction for zenith angle centered at 72.5 degrees, with a range from 70 to 75 degrees.
CRTFCN_CODE	The BOREAS certification level of the data. Examples are CPI (Checked by PI), CGR (Certified by Group), PRE (Preliminary), and CPI-??? (CPI but questionable).
REVISION_DATE	The most recent date when the information in the referenced data base table record was revised.

### 7.3.3 Unit of Measurement

The measurement units for the parameters contained in the data files on the CD-ROM are:

#### CANOPY\_ARCH\_INV

Column Name	Units
SITE_NAME	[none]
SUB_SITE	[none]
DATE_OBS	[DD-MON-YY]
TE23_FILM_ROLL_ID	[none]
BEGIN_PRINT_NUM	[unitless]
END_PRINT_NUM	[unitless]
CD1_ID	[none]
CD2_ID	[none]
BEGIN_CD1_IMAGE_NUM	[unitless]
END_CD1_IMAGE_NUM	[unitless]
PHOTO_QUALITY	[none]
ANALYSIS_STATUS	[none]
COMMENTS	[none]
CRTFCN_CODE	[none]
REVISION_DATE	[DD-MON-YY]

#### CANOPY\_ARCH\_DATA

Column Name	Units
SITE_NAME	[none]
SUB_SITE	[none]
DATE_OBS	[DD-MON-YY]
TE23_FILM_ROLL_ID	[none]
TE23_PHOTO_ID	[none]
TE_X_GRID	[meters]
TE_Y_GRID	[meters]

PHOTO_LOCATION	[none]
MEAN_PHOTO_HT_AGL	[meters]
LEAF_AREA_INDX_EFFEC	[unitless]
EXTINCT_COEF_0_TO_15	[unitless]
EXTINCT_COEF_15_TO_30	[unitless]
EXTINCT_COEF_30_TO_45	[unitless]
EXTINCT_COEF_45_TO_60	[unitless]
EXTINCT_COEF_60_TO_75	[unitless]
LEAF_AREA_0_TO_15	[unitless]
LEAF_AREA_15_TO_30	[unitless]
LEAF_AREA_30_TO_45	[unitless]
LEAF_AREA_45_TO_60	[unitless]
LEAF_AREA_60_TO_75	[unitless]
MEAN_TIP_ANG	[degrees]
STD_ERR_TIP_ANG	[percent]
SKYVIEW_FACTOR	[unitless]
CLUMP_FACTOR	[unitless]
LEAF_AREA_INDX	[unitless]
INDIR_SITE_FACT_NOCOS	[unitless]
INDIR_SITE_FACT_COS	[unitless]
DIR_SITE_FACT_NOCOS	[unitless]
DIR_SITE_FACT_COS	[unitless]
FIPAR_DIF	[unitless]
FIPAR_DIR_YEAR	[unitless]
FIPAR_JUN	[unitless]
FIPAR_JUL_OR_MAY	[unitless]
FIPAR_AUG_OR_APR	[unitless]
FIPAR_SEP_OR_MAR	[unitless]
FIPAR_OCT_OR_FEB	[unitless]
FIPAR_NOV_OR_JAN	[unitless]
FIPAR_DEC	[unitless]
TE23_IMAGE_ID	[none]
THRESHOLD	[unitless]
CD1_ID	[none]
CD1_IMAGE_NUM	[unitless]
CD2_ID	[none]
CD2_IMAGE_NUM	[unitless]
GAP_FRACT_0_TO_5	[unitless]
GAP_FRACT_5_TO_10	[unitless]
GAP_FRACT_10_TO_15	[unitless]
GAP_FRACT_15_TO_20	[unitless]
GAP_FRACT_20_TO_25	[unitless]
GAP_FRACT_25_TO_30	[unitless]
GAP_FRACT_30_TO_35	[unitless]
GAP_FRACT_35_TO_40	[unitless]
GAP_FRACT_40_TO_45	[unitless]
GAP_FRACT_45_TO_50	[unitless]
GAP_FRACT_50_TO_55	[unitless]
GAP_FRACT_55_TO_60	[unitless]
GAP_FRACT_60_TO_65	[unitless]
GAP_FRACT_65_TO_70	[unitless]
GAP_FRACT_70_TO_75	[unitless]
CRTFCN_CODE	[none]
REVISION_DATE	[DD-MON-YY]

**CANOPY\_ARCH\_AVG**

Column Name	Units
SITE_NAME	[none]
SUB_SITE	[none]
DATE_OBS	[DD-MON-YY]
SRC_FILE	[none]
MEAN_PHOTO_HT_AGL	[meters]
NUM_PHOTOS	[counts]
MEAN_LEAF_AREA_INDX	[unitless]
SDEV_LEAF_AREA_INDX	[unitless]
MEAN_LEAF_AREA_INDX_EFFEC	[unitless]
SDEV_LEAF_AREA_INDX_EFFEC	[unitless]
MEAN_EXTINCT_COEF_0_TO_15	[unitless]
SDEV_EXTINCT_COEF_0_TO_15	[unitless]
MEAN_EXTINCT_COEF_15_TO_30	[unitless]
SDEV_EXTINCT_COEF_15_TO_30	[unitless]
MEAN_EXTINCT_COEF_30_TO_45	[unitless]
SDEV_EXTINCT_COEF_30_TO_45	[unitless]
MEAN_EXTINCT_COEF_45_TO_60	[unitless]
SDEV_EXTINCT_COEF_45_TO_60	[unitless]
MEAN_EXTINCT_COEF_60_TO_75	[unitless]
SDEV_EXTINCT_COEF_60_TO_75	[unitless]
MEAN_LEAF_AREA_0_TO_15	[unitless]
SDEV_LEAF_AREA_0_TO_15	[unitless]
MEAN_LEAF_AREA_15_TO_30	[unitless]
SDEV_LEAF_AREA_15_TO_30	[unitless]
MEAN_LEAF_AREA_30_TO_45	[unitless]
SDEV_LEAF_AREA_30_TO_45	[unitless]
MEAN_LEAF_AREA_45_TO_60	[unitless]
SDEV_LEAF_AREA_45_TO_60	[unitless]
MEAN_LEAF_AREA_60_TO_75	[unitless]
SDEV_LEAF_AREA_60_TO_75	[unitless]
MEAN_MEAN_TIP_ANG	[degrees]
SDEV_MEAN_TIP_ANG	[degrees]
MEAN_STD_ERR_TIP_ANG	[percent]
SDEV_STD_ERR_TIP_ANG	[percent]
MEAN_SKYVIEW_FACTOR	[unitless]
SDEV_SKYVIEW_FACTOR	[unitless]
MEAN_INDIR_SITE_FACT_NOCOS	[unitless]
SDEV_INDIR_SITE_FACT_NOCOS	[unitless]
MEAN_INDIR_SITE_FACT_COS	[unitless]
SDEV_INDIR_SITE_FACT_COS	[unitless]
MEAN_DIR_SITE_FACT_NOCOS	[unitless]
SDEV_DIR_SITE_FACT_NOCOS	[unitless]
MEAN_DIR_SITE_FACT_COS	[unitless]
SDEV_DIR_SITE_FACT_COS	[unitless]
MEAN_FIPAR_DIF	[unitless]
SDEV_FIPAR_DIF	[unitless]
MEAN_FIPAR_DIR_YEAR	[unitless]
SDEV_FIPAR_DIR_YEAR	[unitless]
MEAN_FIPAR_JUN	[unitless]
SDEV_FIPAR_JUN	[unitless]
MEAN_FIPAR_JUL_OR_MAY	[unitless]

SDEV_FIPAR_JUL_OR_MAY	[unitless]
MEAN_FIPAR_AUG_OR_APR	[unitless]
SDEV_FIPAR_AUG_OR_APR	[unitless]
MEAN_FIPAR_SEP_OR_MAR	[unitless]
SDEV_FIPAR_SEP_OR_MAR	[unitless]
MEAN_FIPAR_OCT_OR_FEB	[unitless]
SDEV_FIPAR_OCT_OR_FEB	[unitless]
MEAN_FIPAR_NOV_OR_JAN	[unitless]
SDEV_FIPAR_NOV_OR_JAN	[unitless]
MEAN_FIPAR_DEC	[unitless]
SDEV_FIPAR_DEC	[unitless]
MEAN_GAP_FRACT_0_TO_5	[unitless]
SDEV_GAP_FRACT_0_TO_5	[unitless]
MEAN_GAP_FRACT_5_TO_10	[unitless]
SDEV_GAP_FRACT_5_TO_10	[unitless]
MEAN_GAP_FRACT_10_TO_15	[unitless]
SDEV_GAP_FRACT_10_TO_15	[unitless]
MEAN_GAP_FRACT_15_TO_20	[unitless]
SDEV_GAP_FRACT_15_TO_20	[unitless]
MEAN_GAP_FRACT_20_TO_25	[unitless]
SDEV_GAP_FRACT_20_TO_25	[unitless]
MEAN_GAP_FRACT_25_TO_30	[unitless]
SDEV_GAP_FRACT_25_TO_30	[unitless]
MEAN_GAP_FRACT_30_TO_35	[unitless]
SDEV_GAP_FRACT_30_TO_35	[unitless]
MEAN_GAP_FRACT_35_TO_40	[unitless]
SDEV_GAP_FRACT_35_TO_40	[unitless]
MEAN_GAP_FRACT_40_TO_45	[unitless]
SDEV_GAP_FRACT_40_TO_45	[unitless]
MEAN_GAP_FRACT_45_TO_50	[unitless]
SDEV_GAP_FRACT_45_TO_50	[unitless]
MEAN_GAP_FRACT_50_TO_55	[unitless]
SDEV_GAP_FRACT_50_TO_55	[unitless]
MEAN_GAP_FRACT_55_TO_60	[unitless]
SDEV_GAP_FRACT_55_TO_60	[unitless]
MEAN_GAP_FRACT_60_TO_65	[unitless]
SDEV_GAP_FRACT_60_TO_65	[unitless]
MEAN_GAP_FRACT_65_TO_70	[unitless]
SDEV_GAP_FRACT_65_TO_70	[unitless]
MEAN_GAP_FRACT_70_TO_75	[unitless]
SDEV_GAP_FRACT_70_TO_75	[unitless]
CRTFCN_CODE	[none]
REVISION_DATE	[DD-MON-YY]



### 7.3.4 Data Source

The sources of the parameter values contained in the data files on the CD-ROM are:

#### CANOPY\_ARCH\_INV

Column Name	Data Source
SITE_NAME	[BORIS Designation]
SUB_SITE	[BORIS Designation]
DATE_OBS	[Human Observer]
TE23_FILM_ROLL_ID	[Human Observer]
BEGIN_PRINT_NUM	[Human Observer]
END_PRINT_NUM	[Human Observer]
CD1_ID	[Human Observer]
CD2_ID	[Human Observer]
BEGIN_CD1_IMAGE_NUM	[Human Observer]
END_CD1_IMAGE_NUM	[Human Observer]
PHOTO_QUALITY	[Human Observer]
ANALYSIS_STATUS	[Human Observer]
COMMENTS	[Human Observer]
CRTFCN_CODE	[BORIS Designation]
REVISION_DATE	[BORIS Designation]

#### CANOPY\_ARCH\_DATA

Column Name	Data Source
SITE_NAME	[BORIS Designation]
SUB_SITE	[BORIS Designation]
DATE_OBS	[Human Observer]
TE23_FILM_ROLL_ID	[Human Observer]
TE23_PHOTO_ID	[Human Observer]
TE_X_GRID	[Human Observer]
TE_Y_GRID	[Human Observer]
PHOTO_LOCATION	[Human Observer]
MEAN_PHOTO_HT_AGL	[Laboratory Equipment]
LEAF_AREA_INDX_EFFEC	[Laboratory Equipment]
EXTINCT_COEF_0_TO_15	[Laboratory Equipment]
EXTINCT_COEF_15_TO_30	[Laboratory Equipment]
EXTINCT_COEF_30_TO_45	[Laboratory Equipment]
EXTINCT_COEF_45_TO_60	[Laboratory Equipment]
EXTINCT_COEF_60_TO_75	[Laboratory Equipment]
LEAF_AREA_0_TO_15	[Laboratory Equipment]
LEAF_AREA_15_TO_30	[Laboratory Equipment]
LEAF_AREA_30_TO_45	[Laboratory Equipment]
LEAF_AREA_45_TO_60	[Laboratory Equipment]
LEAF_AREA_60_TO_75	[Laboratory Equipment]
MEAN_TIP_ANG	[Laboratory Equipment]
STD_ERR_TIP_ANG	[Laboratory Equipment]
SKYVIEW_FACTOR	[Laboratory Equipment]
CLUMP_FACTOR	[Laboratory Equipment]
LEAF_AREA_INDX	[Laboratory Equipment]
INDIR_SITE_FACT_NOCOS	[Laboratory Equipment]
INDIR_SITE_FACT_COS	[Laboratory Equipment]
DIR_SITE_FACT_NOCOS	[Laboratory Equipment]
DIR_SITE_FACT_COS	[Laboratory Equipment]

FIPAR_DIF	[Laboratory Equipment]
FIPAR_DIR_YEAR	[Laboratory Equipment]
FIPAR_JUN	[Laboratory Equipment]
FIPAR_JUL_OR_MAY	[Laboratory Equipment]
FIPAR_AUG_OR_APR	[Laboratory Equipment]
FIPAR_SEP_OR_MAR	[Laboratory Equipment]
FIPAR_OCT_OR_FEB	[Laboratory Equipment]
FIPAR_NOV_OR_JAN	[Laboratory Equipment]
FIPAR_DEC	[Laboratory Equipment]
TE23_IMAGE_ID	[Human Observer]
THRESHOLD	[Human Observer]
CD1_ID	[Human Observer]
CD1_IMAGE_NUM	[Human Observer]
CD2_ID	[Human Observer]
CD2_IMAGE_NUM	[Human Observer]
GAP_FRACT_0_TO_5	[Laboratory Equipment]
GAP_FRACT_5_TO_10	[Laboratory Equipment]
GAP_FRACT_10_TO_15	[Laboratory Equipment]
GAP_FRACT_15_TO_20	[Laboratory Equipment]
GAP_FRACT_20_TO_25	[Laboratory Equipment]
GAP_FRACT_25_TO_30	[Laboratory Equipment]
GAP_FRACT_30_TO_35	[Laboratory Equipment]
GAP_FRACT_35_TO_40	[Laboratory Equipment]
GAP_FRACT_40_TO_45	[Laboratory Equipment]
GAP_FRACT_45_TO_50	[Laboratory Equipment]
GAP_FRACT_50_TO_55	[Laboratory Equipment]
GAP_FRACT_55_TO_60	[Laboratory Equipment]
GAP_FRACT_60_TO_65	[Laboratory Equipment]
GAP_FRACT_65_TO_70	[Laboratory Equipment]
GAP_FRACT_70_TO_75	[Laboratory Equipment]
CRTFCN_CODE	[BORIS Designation]
REVISION_DATE	[BORIS Designation]

**CANOPY\_ARCH\_AVG**

Column Name	Data Source
SITE_NAME	[BORIS Designation]
SUB_SITE	[BORIS Designation]
DATE_OBS	[Human Observer]
SRC_FILE	[Human Observer]
MEAN_PHOTO_HT_AGL	[Laboratory Equipment]
NUM_PHOTOS	[Human Observer]
MEAN_LEAF_AREA_INDX	[Laboratory Equipment]
SDEV_LEAF_AREA_INDX	[Laboratory Equipment]
MEAN_LEAF_AREA_INDX_EFFEC	[Laboratory Equipment]
SDEV_LEAF_AREA_INDX_EFFEC	[Laboratory Equipment]
MEAN_EXTINCT_COEF_0_TO_15	[Laboratory Equipment]
SDEV_EXTINCT_COEF_0_TO_15	[Laboratory Equipment]
MEAN_EXTINCT_COEF_15_TO_30	[Laboratory Equipment]
SDEV_EXTINCT_COEF_15_TO_30	[Laboratory Equipment]
MEAN_EXTINCT_COEF_30_TO_45	[Laboratory Equipment]
SDEV_EXTINCT_COEF_30_TO_45	[Laboratory Equipment]
MEAN_EXTINCT_COEF_45_TO_60	[Laboratory Equipment]
SDEV_EXTINCT_COEF_45_TO_60	[Laboratory Equipment]

MEAN_EXTINCT_COEF_60_TO_75	[Laboratory Equipment]
SDEV_EXTINCT_COEF_60_TO_75	[Laboratory Equipment]
MEAN_LEAF_AREA_0_TO_15	[Laboratory Equipment]
SDEV_LEAF_AREA_0_TO_15	[Laboratory Equipment]
MEAN_LEAF_AREA_15_TO_30	[Laboratory Equipment]
SDEV_LEAF_AREA_15_TO_30	[Laboratory Equipment]
MEAN_LEAF_AREA_30_TO_45	[Laboratory Equipment]
SDEV_LEAF_AREA_30_TO_45	[Laboratory Equipment]
MEAN_LEAF_AREA_45_TO_60	[Laboratory Equipment]
SDEV_LEAF_AREA_45_TO_60	[Laboratory Equipment]
MEAN_LEAF_AREA_60_TO_75	[Laboratory Equipment]
SDEV_LEAF_AREA_60_TO_75	[Laboratory Equipment]
MEAN_MEAN_TIP_ANG	[Laboratory Equipment]
SDEV_MEAN_TIP_ANG	[Laboratory Equipment]
MEAN_STD_ERR_TIP_ANG	[Laboratory Equipment]
SDEV_STD_ERR_TIP_ANG	[Laboratory Equipment]
MEAN_SKYVIEW_FACTOR	[Laboratory Equipment]
SDEV_SKYVIEW_FACTOR	[Laboratory Equipment]
MEAN_INDIR_SITE_FACT_NOCOS	[Laboratory Equipment]
SDEV_INDIR_SITE_FACT_NOCOS	[Laboratory Equipment]
MEAN_INDIR_SITE_FACT_COS	[Laboratory Equipment]
SDEV_INDIR_SITE_FACT_COS	[Laboratory Equipment]
MEAN_DIR_SITE_FACT_NOCOS	[Laboratory Equipment]
SDEV_DIR_SITE_FACT_NOCOS	[Laboratory Equipment]
MEAN_DIR_SITE_FACT_COS	[Laboratory Equipment]
SDEV_DIR_SITE_FACT_COS	[Laboratory Equipment]
MEAN_FIPAR_DIF	[Laboratory Equipment]
SDEV_FIPAR_DIF	[Laboratory Equipment]
MEAN_FIPAR_DIR_YEAR	[Laboratory Equipment]
SDEV_FIPAR_DIR_YEAR	[Laboratory Equipment]
MEAN_FIPAR_JUN	[Laboratory Equipment]
SDEV_FIPAR_JUN	[Laboratory Equipment]
MEAN_FIPAR_JUL_OR_MAY	[Laboratory Equipment]
SDEV_FIPAR_JUL_OR_MAY	[Laboratory Equipment]
MEAN_FIPAR_AUG_OR_APR	[Laboratory Equipment]
SDEV_FIPAR_AUG_OR_APR	[Laboratory Equipment]
MEAN_FIPAR_SEP_OR_MAR	[Laboratory Equipment]
SDEV_FIPAR_SEP_OR_MAR	[Laboratory Equipment]
MEAN_FIPAR_OCT_OR_FEB	[Laboratory Equipment]
SDEV_FIPAR_OCT_OR_FEB	[Laboratory Equipment]
MEAN_FIPAR_NOV_OR_JAN	[Laboratory Equipment]
SDEV_FIPAR_NOV_OR_JAN	[Laboratory Equipment]
MEAN_FIPAR_DEC	[Laboratory Equipment]
SDEV_FIPAR_DEC	[Laboratory Equipment]
MEAN_GAP_FRACT_0_TO_5	[Laboratory Equipment]
SDEV_GAP_FRACT_0_TO_5	[Laboratory Equipment]
MEAN_GAP_FRACT_5_TO_10	[Laboratory Equipment]
SDEV_GAP_FRACT_5_TO_10	[Laboratory Equipment]
MEAN_GAP_FRACT_10_TO_15	[Laboratory Equipment]
SDEV_GAP_FRACT_10_TO_15	[Laboratory Equipment]
MEAN_GAP_FRACT_15_TO_20	[Laboratory Equipment]
SDEV_GAP_FRACT_15_TO_20	[Laboratory Equipment]
MEAN_GAP_FRACT_20_TO_25	[Laboratory Equipment]
SDEV_GAP_FRACT_20_TO_25	[Laboratory Equipment]

MEAN_GAP_FRACT_25_TO_30	[Laboratory Equipment]
SDEV_GAP_FRACT_25_TO_30	[Laboratory Equipment]
MEAN_GAP_FRACT_30_TO_35	[Laboratory Equipment]
SDEV_GAP_FRACT_30_TO_35	[Laboratory Equipment]
MEAN_GAP_FRACT_35_TO_40	[Laboratory Equipment]
SDEV_GAP_FRACT_35_TO_40	[Laboratory Equipment]
MEAN_GAP_FRACT_40_TO_45	[Laboratory Equipment]
SDEV_GAP_FRACT_40_TO_45	[Laboratory Equipment]
MEAN_GAP_FRACT_45_TO_50	[Laboratory Equipment]
SDEV_GAP_FRACT_45_TO_50	[Laboratory Equipment]
MEAN_GAP_FRACT_50_TO_55	[Laboratory Equipment]
SDEV_GAP_FRACT_50_TO_55	[Laboratory Equipment]
MEAN_GAP_FRACT_55_TO_60	[Laboratory Equipment]
SDEV_GAP_FRACT_55_TO_60	[Laboratory Equipment]
MEAN_GAP_FRACT_60_TO_65	[Laboratory Equipment]
SDEV_GAP_FRACT_60_TO_65	[Laboratory Equipment]
MEAN_GAP_FRACT_65_TO_70	[Laboratory Equipment]
SDEV_GAP_FRACT_65_TO_70	[Laboratory Equipment]
MEAN_GAP_FRACT_70_TO_75	[Laboratory Equipment]
SDEV_GAP_FRACT_70_TO_75	[Laboratory Equipment]
CRTFCN_CODE	[BORIS Designation]
REVISION_DATE	[BORIS Designation]

### 7.3.5 Data Range

The following table gives information about the parameter values found in the data files on the CD-ROM.

#### CANOPY\_ARCH\_INV

Column Name	Minimum Data Value	Maximum Data Value	Missng Data Value	Unrel Data Value	Below Detect Limit	Data Not Cllected
SITE_NAME	NSA-9BS-9TETR	SSA-YJP-FLXTR	None	None	None	None
SUB_SITE	9TE23-HPH00	9TE23-HPH01	None	None	None	None
DATE_OBS	02-MAY-94	26-SEP-94	None	None	None	None
TE23_FILM_ROLL_ID	d1	w6	None	None	None	None
BEGIN_PRINT_NUM	1	1627	None	None	None	None
END_PRINT_NUM	14	1662	None	None	None	None
CD1_ID	115	1851	None	None	None	None
CD2_ID	106	1849	None	None	None	None
BEGIN_CD1_IMAGE_NUM	1	107	None	None	None	None
END_CD1_IMAGE_NUM	4	111	None	None	None	None
PHOTO_QUALITY	N/A	N/A	None	None	None	None
ANALYSIS_STATUS	N/A	N/A	None	None	None	None
COMMENTS	N/A	N/A	-999	None	None	None
CRTFCN_CODE	CPI	CPI	None	None	None	None
REVISION_DATE	10-DEC-98	10-DEC-98	None	None	None	None

## CANOPY\_ARCH\_DATA

Column Name	Minimum Data Value	Maximum Data Value	Missng Data Value	Unrel Data Value	Below Detect Limit	Data Not Cllected
SITE_NAME	NSA-9BS-9TETR	SSA-YJP-FLXTR	None	None	None	None
SUB_SITE	9TE23-HPH00	9TE23-HPH04	None	None	None	None
DATE_OBS	02-MAY-94	17-AUG-94	None	None	None	None
TE23_FILM_ROLL_ID	D01	n11	None	None	None	None
TE23_PHOTO_ID	1	1559	None	None	None	None
TE_X_GRID	-20	200	-999	None	None	None
TE_Y_GRID	-20	30	-999	None	None	None
PHOTO_LOCATION	1	q219	-999	None	None	None
MEAN_PHOTO_HT_AGL	.3	3.5	None	None	None	None
LEAF_AREA_INDX_EFFEC	0	5.1	None	None	None	None
EXTINCT_COEF_0_TO_15	0	2.107	None	None	None	None
EXTINCT_COEF_15_TO_30	0	1.358	None	None	None	None
EXTINCT_COEF_30_TO_45	0	1.178	None	None	None	None
EXTINCT_COEF_45_TO_60	0	1.448	None	None	None	None
EXTINCT_COEF_60_TO_75	.6	2.767	None	None	None	None
LEAF_AREA_0_TO_15	0	.459	None	None	None	None
LEAF_AREA_15_TO_30	.003	.321	None	None	None	None
LEAF_AREA_30_TO_45	0	.553	None	None	None	None
LEAF_AREA_45_TO_60	.006	.482	None	None	None	None
LEAF_AREA_60_TO_75	0	.894	None	None	None	None
MEAN_TIP_ANG	55.463	57.496	None	None	None	None
STD_ERR_TIP_ANG	.357	1.155	None	None	None	None
SKYVIEW_FACTOR	.045	.9322	None	None	None	None
CLUMP_FACTOR	.7	.95	-999	None	None	None
LEAF_AREA_INDX	.016	7.08	-999	None	None	None
INDIR_SITE_FACT_NOCOS	.0271	.9101	None	None	None	None
INDIR_SITE_FACT_COS	.0453	.9851	None	None	None	None
DIR_SITE_FACT_NOCOS	.0051	.9555	None	None	None	None
DIR_SITE_FACT_COS	.0054	.9391	None	None	None	None
FIPAR_DIF	.0149	.9547	None	None	None	None
FIPAR_DIR_YEAR	.061	.995	None	None	None	None
FIPAR_JUN	.0009	1	None	None	None	None
FIPAR_JUL_OR_MAY	.0008	.9943	None	None	None	None
FIPAR_AUG_OR_APR	.0003	.9956	None	None	None	None
FIPAR_SEP_OR_MAR	.0007	.9999	None	None	None	None
FIPAR_OCT_OR_FEB	.4239	1	None	None	None	None
FIPAR_NOV_OR_JAN	.0071	1	None	None	None	None
FIPAR_DEC	.0131	1	None	None	None	None
TE23_IMAGE_ID	N13#0572.IMG	s34#1175.img	None	None	None	None
THRESHOLD	40	114	None	None	None	None
CD1_ID	120	1851	None	None	None	None
CD1_IMAGE_NUM	1	110	None	None	None	None
CD2_ID	114	1849	None	None	None	None
CD2_IMAGE_NUM	1	110	None	None	None	None

GAP_FRACT_0_TO_5	0	1	None	None	None	None
GAP_FRACT_5_TO_10	.0111	1	None	None	None	None
GAP_FRACT_10_TO_15	.0157	1	None	None	None	None
GAP_FRACT_15_TO_20	.0193	1	None	None	None	None
GAP_FRACT_20_TO_25	.0135	1	None	None	None	None
GAP_FRACT_25_TO_30	.0435	1	None	None	None	None
GAP_FRACT_30_TO_35	.0581	1	None	None	None	None
GAP_FRACT_35_TO_40	.0205	1	None	None	None	None
GAP_FRACT_40_TO_45	.031	1	None	None	None	None
GAP_FRACT_45_TO_50	.0205	1	None	None	None	None
GAP_FRACT_50_TO_55	.0029	1	None	None	None	None
GAP_FRACT_55_TO_60	.0036	1	None	None	None	None
GAP_FRACT_60_TO_65	.0003	.9968	None	None	None	None
GAP_FRACT_65_TO_70	0	.9945	None	None	None	None
GAP_FRACT_70_TO_75	0	.9794	None	None	None	None
CRTFCN_CODE	CPI	CPI	None	None	None	None
REVISION_DATE	16-DEC-98	16-DEC-98	None	None	None	None

**CANOPY\_ARCH\_AVG**

Column Name	Minimum Data Value	Maximum Data Value	Missng Data Value	Unrel Data Value	Below Detect Limit	Data Not Clcltd
SITE_NAME	NSA-9BS-9TETR	SSA-YJP-FLXTR	None	None	None	None
SUB_SITE	9TE23-HPH00	9TE23-HPH01	None	None	None	None
DATE_OBS	02-MAY-94	17-AUG-94	None	None	None	None
SRC_FILE	ANO9P.TXT	CSYJP-.TXT	None	None	None	None
MEAN_PHOTO_HT_AGL	.3	2.5	None	None	None	None
NUM_PHOTOS	3	25	None	None	None	None
MEAN_LEAF_AREA_INDX	.18	5.69	-999	None	None	None
SDEV_LEAF_AREA_INDX	.121	1.153	-999	None	None	None
MEAN_LEAF_AREA_INDX_	.056	4.096	None	None	None	None
EFFEC						
SDEV_LEAF_AREA_INDX_	.061	.83	None	None	None	None
EFFEC						
MEAN_EXTINCT_COEF_0_	0	.629	None	None	None	None
TO_15						
SDEV_EXTINCT_COEF_0_	0	.702	None	None	None	None
TO_15						
MEAN_EXTINCT_COEF_15_	.054	.614	None	None	None	None
TO_30						
SDEV_EXTINCT_COEF_15_	.023	.489	None	None	None	None
TO_30						
MEAN_EXTINCT_COEF_30_	.138	.694	None	None	None	None
TO_45						
SDEV_EXTINCT_COEF_30_	.004	.421	None	None	None	None
TO_45						
MEAN_EXTINCT_COEF_45_	.547	.972	None	None	None	None
TO_60						
SDEV_EXTINCT_COEF_45_	.003	.502	None	None	None	None
TO_60						
MEAN_EXTINCT_COEF_60_	1.261	2.179	None	None	None	None
TO_75						

SDEV_EXTINCT_COEF_60_	.019	.674	None	None	None	None
TO_75						
MEAN_LEAF_AREA_0_TO_	0	.144	None	None	None	None
15						
SDEV_LEAF_AREA_0_TO_	0	.226	None	None	None	None
15						
MEAN_LEAF_AREA_15_TO_	.053	.167	None	None	None	None
30						
SDEV_LEAF_AREA_15_TO_	0	.115	None	None	None	None
30						
MEAN_LEAF_AREA_30_TO_	.055	.299	None	None	None	None
45						
SDEV_LEAF_AREA_30_TO_	0	.171	None	None	None	None
45						
MEAN_LEAF_AREA_45_TO_	.198	.333	None	None	None	None
60						
SDEV_LEAF_AREA_45_TO_	0	.16	None	None	None	None
60						
MEAN_LEAF_AREA_60_TO_	.157	.564	None	None	None	None
75						
SDEV_LEAF_AREA_60_TO_	0	.238	None	None	None	None
75						
MEAN_MEAN_TIP_ANG	56.72	57.43	None	None	None	None
SDEV_MEAN_TIP_ANG	.026	.67	None	None	None	None
MEAN_STD_ERR_TIP_ANG	.382	.664	None	None	None	None
SDEV_STD_ERR_TIP_ANG	.008	.252	None	None	None	None
MEAN_SKYVIEW_FACTOR	.1036	.8988	None	None	None	None
SDEV_SKYVIEW_FACTOR	.0121	.2394	None	None	None	None
MEAN_INDIR_SITE_FACT_	.0622	.8656	None	None	None	None
NOCOS						
SDEV_INDIR_SITE_FACT_	.008	.2289	None	None	None	None
NOCOS						
MEAN_INDIR_SITE_FACT_	.104	.9474	None	None	None	None
COS						
SDEV_INDIR_SITE_FACT_	.0122	.2498	None	None	None	None
COS						
MEAN_DIR_SITE_FACT_	.0462	.9026	None	None	None	None
NOCOS						
SDEV_DIR_SITE_FACT_	.0135	.2956	None	None	None	None
NOCOS						
MEAN_DIR_SITE_FACT_	.0572	.8964	None	None	None	None
COS						
SDEV_DIR_SITE_FACT_	.0166	.274	None	None	None	None
COS						
MEAN_FIPAR_DIF	.0526	.896	None	None	None	None
SDEV_FIPAR_DIF	.0122	.2498	None	None	None	None
MEAN_FIPAR_DIR_YEAR	.1036	.9428	None	None	None	None
SDEV_FIPAR_DIR_YEAR	.0166	.274	None	None	None	None
MEAN_FIPAR_JUN	.02	.902	None	None	None	None
SDEV_FIPAR_JUN	.0348	.3064	None	None	None	None
MEAN_FIPAR_JUL_OR_	.0178	.9248	None	None	None	None
MAY						
SDEV_FIPAR_JUL_OR_	.0185	.2887	None	None	None	None
MAY						

MEAN_FIPAR_AUG_OR_	.0159	.945	None	None	None	None
APR						
SDEV_FIPAR_AUG_OR_	.0205	.315	None	None	None	None
APR						
MEAN_FIPAR_SEP_OR_	.0352	.9816	None	None	None	None
MAR						
SDEV_FIPAR_SEP_OR_	.0149	.3624	None	None	None	None
MAR						
MEAN_FIPAR_OCT_OR_	.5442	.998	None	None	None	None
FEB						
SDEV_FIPAR_OCT_OR_	.0017	.1865	None	None	None	None
FEB						
MEAN_FIPAR_NOV_OR_	.1651	1	None	None	None	None
JAN						
SDEV_FIPAR_NOV_OR_	0	.4143	None	None	None	None
JAN						
MEAN_FIPAR_DEC	.1251	1	None	None	None	None
SDEV_FIPAR_DEC	0	.4337	None	None	None	None
MEAN_GAP_FRACT_0_TO_	.2694	1	None	None	None	None
5						
SDEV_GAP_FRACT_0_TO_	0	.4414	None	None	None	None
5						
MEAN_GAP_FRACT_5_TO_	.2182	1	None	None	None	None
10						
SDEV_GAP_FRACT_5_TO_	0	.356	None	None	None	None
10						
MEAN_GAP_FRACT_10_TO_	.2204	1	None	None	None	None
15						
SDEV_GAP_FRACT_10_TO_	0	.3545	None	None	None	None
15						
MEAN_GAP_FRACT_15_TO_	.1863	.9968	None	None	None	None
20						
SDEV_GAP_FRACT_15_TO_	.0096	.3352	None	None	None	None
20						
MEAN_GAP_FRACT_20_TO_	.1778	.9927	None	None	None	None
25						
SDEV_GAP_FRACT_20_TO_	.0208	.3384	None	None	None	None
25						
MEAN_GAP_FRACT_25_TO_	.1679	.9859	None	None	None	None
30						
SDEV_GAP_FRACT_25_TO_	.0244	.3069	None	None	None	None
30						
MEAN_GAP_FRACT_30_TO_	.1638	.98	None	None	None	None
35						
SDEV_GAP_FRACT_30_TO_	.0249	.2617	None	None	None	None
35						
MEAN_GAP_FRACT_35_TO_	.1165	.9773	None	None	None	None
40						
SDEV_GAP_FRACT_35_TO_	.0196	.2447	None	None	None	None
40						
MEAN_GAP_FRACT_40_TO_	.0883	.9734	None	None	None	None
45						
SDEV_GAP_FRACT_40_TO_	.0136	.2442	None	None	None	None
45						



MEAN_GAP_FRACT_45_TO_50	.0595	.9654	None	None	None	None
SDEV_GAP_FRACT_45_TO_50	.0108	.2502	None	None	None	None
MEAN_GAP_FRACT_50_TO_55	.0353	.9729	None	None	None	None
SDEV_GAP_FRACT_50_TO_55	.0119	.2589	None	None	None	None
MEAN_GAP_FRACT_55_TO_60	.0128	.9669	None	None	None	None
SDEV_GAP_FRACT_55_TO_60	.0122	.2617	None	None	None	None
MEAN_GAP_FRACT_60_TO_65	.0048	.9585	None	None	None	None
SDEV_GAP_FRACT_60_TO_65	.0039	.2747	None	None	None	None
MEAN_GAP_FRACT_65_TO_70	.0011	.9477	None	None	None	None
SDEV_GAP_FRACT_65_TO_70	.0009	.3134	None	None	None	None
MEAN_GAP_FRACT_70_TO_75	.0002	.9296	None	None	None	None
SDEV_GAP_FRACT_70_TO_75	.0003	.3458	None	None	None	None
CRTFCN_CODE	CPI	CPI	None	None	None	None
REVISION_DATE	16-DEC-98	16-DEC-98	None	None	None	None

-----

Minimum Data Value -- The minimum value found in the column.  
Maximum Data Value -- The maximum value found in the column.  
Missng Data Value -- The value that indicates missing data. This is used to indicate that an attempt was made to determine the parameter value, but the attempt was unsuccessful.  
Unrel Data Value -- The value that indicates unreliable data. This is used to indicate an attempt was made to determine the parameter value, but the value was deemed to be unreliable by the analysis personnel.  
Below Detect Limit -- The value that indicates parameter values below the instruments detection limits. This is used to indicate that an attempt was made to determine the parameter value, but the analysis personnel determined that the parameter value was below the detection limit of the instrumentation.  
Data Not Cllctd -- This value indicates that no attempt was made to determine the parameter value. This usually indicates that BORIS combined several similar but not identical data sets into the same data base table but this particular science team did not measure that parameter.

Blank -- Indicates that blank spaces are used to denote that type of value.  
N/A -- Indicates that the value is not applicable to the respective column.  
None -- Indicates that no values of that sort were found in the column.

-----

## 7.4 Sample Data Record

The following are wrapped versions of data records from a sample data file on the CD-ROM.

### CANOPY\_ARCH\_INV

```
SITE_NAME,SUB_SITE,DATE_OBS,TE23_FILM_ROLL_ID,BEGIN_PRINT_NUM,END_PRINT_NUM,
CD1_ID,CD2_ID,BEGIN_CD1_IMAGE_NUM,END_CD1_IMAGE_NUM,PHOTO_QUALITY,
ANALYSIS_STATUS,COMMENTS,CRTFCN_CODE,REVISION_DATE
'SSA-90A-FLXTR','9TE23-HPH01',02-MAY-94,'j1',1,14,849,377,1,14,'Good','Complete',
'Not_oriented_correctly_(upside_down).','CPI',10-DEC-98
'SSA-90A-FLXTR','9TE23-HPH01',06-MAY-94,'j1',15,36,849,377,15,36,'Good',
'Complete','Not_oriented_correctly_(upside_down).','CPI',10-DEC-98
```

### CANOPY\_ARCH\_DATA

```
SITE_NAME,SUB_SITE,DATE_OBS,TE23_FILM_ROLL_ID,TE23_PHOTO_ID,TE_X_GRID,TE_Y_GRID,
PHOTO_LOCATION,MEAN_PHOTO_HT_AGL,LEAF_AREA_INDX_EFFEC,EXTINCT_COEF_0_TO_15,
EXTINCT_COEF_15_TO_30,EXTINCT_COEF_30_TO_45,EXTINCT_COEF_45_TO_60,
EXTINCT_COEF_60_TO_75,LEAF_AREA_0_TO_15,LEAF_AREA_15_TO_30,LEAF_AREA_30_TO_45,
LEAF_AREA_45_TO_60,LEAF_AREA_60_TO_75,MEAN_TIP_ANG,STD_ERR_TIP_ANG,
SKYVIEW_FACTOR,CLUMP_FACTOR,LEAF_AREA_INDX,INDIR_SITE_FACT_NOCOS,
INDIR_SITE_FACT_COS,DIR_SITE_FACT_NOCOS,DIR_SITE_FACT_COS,FIPAR_DIF,
FIPAR_DIR_YEAR,FIPAR_JUN,FIPAR_JUL_OR_MAY,FIPAR_AUG_OR_APR,FIPAR_SEP_OR_MAR,
FIPAR_OCT_OR_FEB,FIPAR_NOV_OR_JAN,FIPAR_DEC,TE23_IMAGE_ID,THRESHOLD,
CD1_ID,CD1_IMAGE_NUM,CD2_ID,CD2_IMAGE_NUM,GAP_FRACT_0_TO_5,GAP_FRACT_5_TO_10,
GAP_FRACT_10_TO_15,GAP_FRACT_15_TO_20,GAP_FRACT_20_TO_25,GAP_FRACT_25_TO_30,
GAP_FRACT_30_TO_35,GAP_FRACT_35_TO_40,GAP_FRACT_40_TO_45,GAP_FRACT_45_TO_50,
GAP_FRACT_50_TO_55,GAP_FRACT_55_TO_60,GAP_FRACT_60_TO_65,GAP_FRACT_65_TO_70,
GAP_FRACT_70_TO_75,CRTFCN_CODE,REVISION_DATE
'SSA-90A-FLXTR','9TE23-HPH01',02-MAY-94,'J01',1,-999,-999,'1',.5,1.36,.384,.367,
.533,.805,1.476,.001,.073,.204,.328,.394,56.98,.536,.387,.77,1.766,.2646,.3874,
.1247,.1293,.6126,.871,.6996,.8143,.9374,.9751,.9991,.9986,1.0,'j01#0001.img',
85,849,1,377,1,.5306,.5993,.6025,.6197,.587,.6131,.5457,.5091,.4202,.3949,
.357,.2758,.2067,.1491,.0689,'CPI',16-DEC-98
'SSA-90A-FLXTR','9TE23-HPH01',02-MAY-94,'J01',2,-999,-999,'1',1.5,1.0,.53,.557,
.53,.694,1.415,.002,.11,.285,.33,.272,56.801,.599,.467,.77,1.294,.3461,.4702,
.351,.3722,.5298,.628,.4558,.5235,.6029,.7771,.9831,.9995,1.0,'j01#0002.img',
86,849,2,377,2,.4288,.5753,.6313,.5711,.573,.5773,.5787,.6036,.5868,.5521,.5216,
.4406,.3297,.2439,.1752,'CPI',16-DEC-98
```

### CANOPY\_ARCH\_AVG

```
SITE_NAME,SUB_SITE,DATE_OBS,SRC_FILE,MEAN_PHOTO_HT_AGL,NUM_PHOTOS,
MEAN_LEAF_AREA_INDX,SDEV_LEAF_AREA_INDX,MEAN_LEAF_AREA_INDX_EFFEC,
SDEV_LEAF_AREA_INDX_EFFEC,MEAN_EXTINCT_COEF_0_TO_15,SDEV_EXTINCT_COEF_0_TO_15,
MEAN_EXTINCT_COEF_15_TO_30,SDEV_EXTINCT_COEF_15_TO_30,MEAN_EXTINCT_COEF_30_TO_45,
SDEV_EXTINCT_COEF_30_TO_45,MEAN_EXTINCT_COEF_45_TO_60,SDEV_EXTINCT_COEF_45_TO_60,
MEAN_EXTINCT_COEF_60_TO_75,SDEV_EXTINCT_COEF_60_TO_75,MEAN_LEAF_AREA_0_TO_15,
SDEV_LEAF_AREA_0_TO_15,MEAN_LEAF_AREA_15_TO_30,SDEV_LEAF_AREA_15_TO_30,
MEAN_LEAF_AREA_30_TO_45,SDEV_LEAF_AREA_30_TO_45,MEAN_LEAF_AREA_45_TO_60,
SDEV_LEAF_AREA_45_TO_60,MEAN_LEAF_AREA_60_TO_75,SDEV_LEAF_AREA_60_TO_75,
MEAN_MEAN_TIP_ANG,SDEV_MEAN_TIP_ANG,MEAN_STD_ERR_TIP_ANG,SDEV_STD_ERR_TIP_ANG,
MEAN_SKYVIEW_FACTOR,SDEV_SKYVIEW_FACTOR,MEAN_INDIR_SITE_FACT_NOCOS,
SDEV_INDIR_SITE_FACT_NOCOS,MEAN_INDIR_SITE_FACT_COS,SDEV_INDIR_SITE_FACT_COS,
MEAN_DIR_SITE_FACT_NOCOS,SDEV_DIR_SITE_FACT_NOCOS,MEAN_DIR_SITE_FACT_COS,
SDEV_DIR_SITE_FACT_COS,MEAN_FIPAR_DIF,SDEV_FIPAR_DIF,MEAN_FIPAR_DIR_YEAR,
SDEV_FIPAR_DIR_YEAR,MEAN_FIPAR_JUN,SDEV_FIPAR_JUN,MEAN_FIPAR_JUL_OR_MAY,
```

```

SDEV_FIPAR_JUL_OR_MAY,MEAN_FIPAR_AUG_OR_APR,SDEV_FIPAR_AUG_OR_APR,
MEAN_FIPAR_SEP_OR_MAR,SDEV_FIPAR_SEP_OR_MAR,MEAN_FIPAR_OCT_OR_FEB,
SDEV_FIPAR_OCT_OR_FEB,MEAN_FIPAR_NOV_OR_JAN,SDEV_FIPAR_NOV_OR_JAN,
MEAN_FIPAR_DEC,SDEV_FIPAR_DEC,MEAN_GAP_FRACT_0_TO_5,SDEV_GAP_FRACT_0_TO_5,
MEAN_GAP_FRACT_5_TO_10,SDEV_GAP_FRACT_5_TO_10,MEAN_GAP_FRACT_10_TO_15,
SDEV_GAP_FRACT_10_TO_15,MEAN_GAP_FRACT_15_TO_20,SDEV_GAP_FRACT_15_TO_20,
MEAN_GAP_FRACT_20_TO_25,SDEV_GAP_FRACT_20_TO_25,MEAN_GAP_FRACT_25_TO_30,
SDEV_GAP_FRACT_25_TO_30,MEAN_GAP_FRACT_30_TO_35,SDEV_GAP_FRACT_30_TO_35,
MEAN_GAP_FRACT_35_TO_40,SDEV_GAP_FRACT_35_TO_40,MEAN_GAP_FRACT_40_TO_45,
SDEV_GAP_FRACT_40_TO_45,MEAN_GAP_FRACT_45_TO_50,SDEV_GAP_FRACT_45_TO_50,
MEAN_GAP_FRACT_50_TO_55,SDEV_GAP_FRACT_50_TO_55,MEAN_GAP_FRACT_55_TO_60,
SDEV_GAP_FRACT_55_TO_60,MEAN_GAP_FRACT_60_TO_65,SDEV_GAP_FRACT_60_TO_65,
MEAN_GAP_FRACT_65_TO_70,SDEV_GAP_FRACT_65_TO_70,MEAN_GAP_FRACT_70_TO_75,
SDEV_GAP_FRACT_70_TO_75,CRTFCN_CODE,REVISION_DATE
'SSA-90A-FLXTR','9TE23-HPH01',02-MAY-94,'CS-OA1.TXT',2.5,10,1.738,.554,1.338,
.427,.388,.23,.456,.135,.598,.102,.786,.073,1.43,.108,.032,.04,.098,.041,.212,
.102,.297,.046,.361,.149,56.937,.198,.57,.067,.3949,.1037,.279,.0843,.3957,
.1049,.35,.0925,.381,.0934,.6043,.1049,.619,.0934,.5219,.1027,.5337,.0987,
.5877,.0993,.6899,.1276,.919,.0567,.9672,.0384,.9909,.0146,.6693,.2531,.6349,
.1576,.6235,.1491,.6012,.1125,.5721,.1236,.5312,.1434,.507,.1485,.47,.1589,
.4418,.145,.412,.1315,.3839,.1298,.338,.1331,.2774,.1141,.1934,.0983,.0866,
.0765,'CPI',16-DEC-98
'SSA-90A-FLXTR','9TE23-HPH01',02-MAY-94,'CS-OA1.TXT',.5,10,1.595,.336,1.228,
.259,.343,.196,.403,.087,.615,.102,.807,.08,1.445,.09,.033,.049,.085,.028,.18,
.095,.292,.052,.409,.127,56.988,.159,.552,.052,.4151,.0622,.2909,.0502,.4155,
.0624,.3283,.1002,.3529,.11,.5845,.0624,.6471,.11,.5419,.1056,.5644,.1184,
.6316,.1393,.7161,.1443,.9264,.0552,.9671,.0349,.9907,.0128,.6707,.279,.6692,
.1338,.6795,.0929,.6754,.0892,.6262,.0635,.5738,.0712,.5143,.1055,.486,.1049,
.4552,.1055,.4228,.0974,.3961,.093,.3487,.0921,.2859,.0771,.1993,.0646,.0938,
.0428,'CPI',16-DEC-98

```

## 8. Data Organization

### 8.1 Data Granularity

The smallest unit of data tracked by BORIS was the data collected at a given site on a given date.

### 8.2 Data Format

The CD-ROM files contain American Standard Code for Information Interchange (ASCII) numerical and character fields of varying length separated by commas. The character fields are enclosed with single apostrophe marks. There are no spaces between the fields.

Each data file on the CD-ROM has four header lines of Hyper-Text Markup Language (HTML) code at the top. When viewed with a Web browser, this code displays header information (data set title, location, date, acknowledgments, etc.) and a series of HTML links to associated data files and related data sets. Line 5 of each data file is a list of the column names, and line 6 and following lines contain the actual data.

The hemispherical photographs are stored in the original set of 42 CD-ROMs that BORIS received from TE-23 and submitted to ORNL. Contact ORNL for further information regarding the hemispherical photography CD-ROMs.

## **9. Data Manipulations**

### **9.1 Formulae**

#### **9.1.1 Derivation Techniques and Algorithms**

Direct transmitted radiation beneath the canopy was estimated as a direct site factor (DSF), the proportion of direct radiation beneath the canopy assuming clear sky conditions (Rich, 1989, 1990). This is reported as an integrated annual value both without and with a cosine correction for incidence on a horizontal plane (DSFU and DSFC, respectively). In addition, monthly integrated values are reported for direct FIPAR (1-DSFC for the month). Diffuse transmitted radiation beneath the canopy was estimated as an indirect site factor (ISF), the proportion of diffuse radiation beneath the canopy assuming clear sky conditions, an isotropic distribution of incoming diffuse radiation, and reported both without a cosine correction (ISFU) and with a cosine correction for incidence on a horizontal plane (ISFC, equivalent to skyview factor). Diffuse FIPAR is reported as 1-ISFC. Gap fraction, the proportion of unobstructed sky, was calculated at five-degree zenith angle intervals and used for additional calculations.

LAI and other canopy indices were calculated using the program LAICalc. Calculating formulae and operation of LAICalc are described in detail in the LAICalc manual (Rich et al., 1995). Additional explanation of theory is provided in the data documentation for RSS-07 (Jing Chen) and the LAI intercomparison paper (Chen et al., 1997).

### **9.2 Data Processing Sequence**

#### **9.2.1 Processing Steps**

None given.

#### **9.2.2 Processing Changes**

None given.

### **9.3 Calculations**

#### **9.3.1 Special Corrections/Adjustments**

None given.

#### **9.3.2 Calculated Variables**

None given.

### **9.4 Graphs and Plots**

None given.

## **10. Errors**

### **10.1 Sources of Error**

Errors can result from uneven lighting during photograph acquisition, alignment problems during digitization, choice of the threshold for image classification, and operator errors during data entry. We minimized these errors. All of our photos were scored for quality and generally of excellent quality.

### **10.2 Quality Assessment**

### **10.2.1 Data Validation by Source**

Much of our quality control involved data validation while still in the field, retaking when necessary, and noting of any data problems. Hemispherical photograph quality was screened and scored after the film was processed. Further quality control involved checking for out-of-range values and cross-checking correspondence between data base file values and field data notebooks.

### **10.2.2 Confidence Level/Accuracy Judgment**

Overall, our measurements are well within the accuracy necessary for our studies and for the purposes of other BOREAS researchers. We can readily assign quantitative estimates of accuracy with a high level of confidence. See Chen et al., 1997.

### **10.2.3 Measurement Error for Parameters and Variables**

The only error we have for gap fraction and transmittance is with respect to repeatability of analyses. Refer to Chen's calculation of clumping factor for estimates of error for that.

FIPAR error estimate: +/- 15% LAI effective error estimate: +/-20%

### **10.2.4 Additional Quality Assessments**

All data files checked against original field acquisition sheets.

### **10.2.5 Data Verification by Data Center**

Data were examined for general consistency and clarity.

## **11. Notes**

### **11.1 Limitations of the Data**

Hemispherical photographs have inherent limitations related to uneven lighting from the sky and uneven illumination of leaves.

### **11.2 Known Problems with the Data**

Hemispherical photographs scored as poor quality yield more variable results.

### **11.3 Usage Guidance**

As with any data set, caution should be used in the interpretation and application of the data. TE-23 and collaborators have done their best to produce an accurate and useful data set, but do not assume responsibility or liability for the use of these data.

### **11.4 Other Relevant Information**

The hemispherical photographs are stored in the original set of 42 CD-ROMs that BORIS received from TE-23 and submitted to ORNL. Contact ORNL for further information regarding the hemispherical photography CD-ROMs.

BORIS staff excluded one row of data from the extracted Data Inventory files on the CD-ROM due to missing site information. This data row is given below:

```
SITE_NAME , SUB_SITE , DATE_OBS , TE23_FILM_ROLL_ID , BEGIN_PRINT_NUM , END_PRINT_NUM ,  
CD1_ID , CD2_ID , BEGIN_CD1_IMAGE_NUM , END_CD1_IMAGE_NUM , PHOTO_QUALITY ,  
ANALYSIS_STATUS , COMMENTS , CRTFCN_CODE , REVISION_DATE  
N -999 -999 w7 1343 1379 117 132 1 37 Good Incomplete  
No_data_sheets_accompanied_this_roll.
```

The '-999' denotes missing data.

## 12. Application of the Data Set

These hemispherical photographs serve two general categories of applications:

- Modeling applications that require extensive LAI or FIPAR measurements for a broad range of sites; e.g., modeling of whole canopy carbon flux, modeling of influences of canopy geometry on light regimes, and modeling of forest dynamics.
- Field measurement of LAI or FIPAR that require cross checks of values; e.g., field studies of light regime, LAI.

## 13. Future Modifications and Plans

Further work will involve reanalysis of the hemispherical photographs using the new commercial program HemiView, validation of light simulation models, and examination of correspondence between PAR sensor measurements and hemispherical photograph estimates.

## 14. Software

### 14.1 Software Description

Microsoft Excel v.5.x spreadsheets were used for organizing data and performing calculations. Canopy v.2.1 was used for analysis of hemispherical photographs (see Rich 1989, 1990). HemiView 1.0 will be available soon for analysis of hemispherical photographs. LAICalc was used for calculation of LAI.

### 14.2 Software Access

Original Microsoft Excel v.5.x spreadsheets are available upon request from TE-23. Canopy v.2.1 is available from TE-23, but requires specialized hardware to run. HemiView 1.0 will be available commercially from Delta-T Devices Ltd. (Cambridge, England). LAICalc is available from BORIS or TE-23.

## 15. Data Access

The canopy architecture and spectral data are available from the Earth Observing System Data and Information System (EOSDIS) ORNL Distributed Active Archive Center (DAAC).

### 15.1 Contact Information

For BOREAS data and documentation please contact:

ORNL DAAC User Services  
Oak Ridge National Laboratory  
P.O. Box 2008 MS-6407  
Oak Ridge, TN 37831-6407  
Phone: (423) 241-3952  
Fax: (423) 574-4665  
E-mail: ornl~~daac~~@ornl.gov or ornl@eos.nasa.gov

### 15.2 Data Center Identification

Earth Observing System Data and Information System (EOSDIS) Oak Ridge National Laboratory (ORNL) Distributed Active Archive Center (DAAC) for Biogeochemical Dynamics  
<http://www-eosdis.ornl.gov/>.

### **15.3 Procedures for Obtaining Data**

Users may obtain data directly through the ORNL DAAC online search and order system [<http://www-eosdis.ornl.gov/>] and the anonymous FTP site [<ftp://www-eosdis.ornl.gov/data/>] or by contacting User Services by electronic mail, telephone, fax, letter, or personal visit using the contact information in Section 15.1.

### **15.4 Data Center Status/Plans**

The ORNL DAAC is the primary source for BOREAS field measurement, image, GIS, and hardcopy data products. The BOREAS CD-ROM and data referenced or listed in inventories on the CD-ROM are available from the ORNL DAAC.

## **16. Output Products and Availability**

### **16.1 Tape Products**

Eight-mm tapes of digitized video images used in analysis are available from TE-23.

### **16.2 Film Products**

Original negatives are archived and stored at KU by TE-23.

### **16.3 Other Products**

The derived data are available on the BOREAS CD-ROM series.

The hemispherical photograph analysis data set is available in ASCII format from ORNL and on local UNIX or PC computers at KU. Analysis data are also available in Microsoft Excel v.5.0 format.

The hemispherical images are available as video digitized image files (512 x 480 x 8 bits) and in Kodak PhotoCD format and are available through KU.

The hemispherical photographs are stored in the original set of 42 CD-ROMs that BORIS received from TE-23 and submitted to ORNL. Contact ORNL for further information regarding the hemispherical photography CD-ROMs.

## **17. References**

### **17.1 Platform/Sensor/Instrument/Data Processing Documentation**

CID. 1995. Plant canopy analyzer CI-100 manual. CID, Incorporated. Vancouver, WA.

Decagon. 1994. Sunfleck ceptometer manual. Decagon, Inc. Pullman, WA.

LI-COR. 1991. LAI-2000 plant canopy analyzer operating manual. LI-COR, Inc. Lincoln, NE.

### **17.2 Journal Articles and Study Reports**

Anderson, M.C. 1964. Studies of the woodland light climate I. The photographic computation of light condition. *Journal of Ecology* 52:27-41.

Anderson, M.C. 1971. Radiation and crop structure. pp. 77-90. In: Z. Sestak, J. Catsky and P.G. Jarvis (eds.). *Plant Photosynthetic Production Manual of Methods*. Junk. The Hague.

Becker, P., D.W. Erhart, and A.P. Smith. 1989. Analysis of forest light environments. 1. Computerized estimation of solar-radiation from hemispherical canopy photographs. *Agricultural and Forest Meteorology* 44: (3-4) 217-232.

Bonhomme, R., C. Varlet Granger, and P. Chartier. 1974. The use of hemispherical photographs for determining the leaf area index of young crops. *Photosynthetica* 8:299-301.

- Canham, C.D., J.S. Denslow, W.J. Platt, J.R. Runkle, T.A. Spies, and P.S. White. 1990. Light regimes beneath closed canopies and tree-fall gaps in temperate and tropical forests. *Canadian Journal of Forest Research* 20: (5) 620-631.
- Chazdon R.L. and C.B. Field. 1987. Photographic estimation of photosynthetically active radiation - evaluation of a computerized technique. *Oecologia* 73: (4) 525-532.
- Chen, J.M. and J. Cihlar. 1995. Plant canopy gap size analysis theory for improving optical measurements of leaf area index. *Applied Optics* 34:(27) 6211-6222.
- Chen, J.M. and T.A. Black. 1992. Defining leaf area index for non-flat leaves. *Plant, Cell and Environment* 15:421-429.
- Chen, J.M., P.M. Rich, S.T. Gower, J.M. Norman, and S. Plummer. 1997. Leaf area index of boreal forests: Theory, techniques, and measurements. *Journal of Geophysical Research* 102 (D24), 29,429-29,443.
- Chen, J.M., T.A. Black, and R.S. Adams. 1991. Evaluation of hemispherical photography for determining plant area index and geometry of a forest stand. *Agricultural and Forest Meteorology* 56:129-143.
- Clark, D.B., D.A. Clark, P.M. Rich, S.B. Weiss, and S.F. Oberbauer. 1996. Landscape-scale evaluation of understory light and canopy structure: Methods and application in a neotropical lowland rain forest. *Canadian Journal of Forest Research* 26:747-757.
- Evans, G.D. and D.E. Coombe. 1959. Hemispherical and woodland canopy photography and the light climate. *Journal of Ecology* 47:103-113.
- Fournier, R.A., P.M. Rich, and R. Landry. 1997. Hierarchical characterization of canopy architecture for boreal forest. *Journal of Geophysical Research* 102 (D24), 29,445-29,454.
- Fournier, R.A., P.M. Rich, Y.R. Alger, V.L. Peterson, R. Landry, and N.M. August. 1995. Canopy architecture of boreal forest: links between remote sensing and ecology. *American Society for Photogrammetry and Remote Sensing Technical Papers* 2:225-235.
- Fournier, R.A., R. Landry, N.M. August, G. Fedosejevs, and R.P. Gauthier. 1996. Modeling light obstruction in three conifer forests using hemispherical photography and fine tree architecture. *Agricultural Forest Meteorology* 82:47-72.
- Galo, A.T., P.M. Rich, and J.J. Ewel. 1992. Effects of forest edges on the solar radiation regime in a series of reconstructed tropical ecosystems. *American Society for Photogrammetry and Remote Sensing Technical Papers*, pp. 98-108.
- Gower, S.T. and J.M. Norman. 1991. Rapid estimation of leaf area index in forests using the LI-COR LAI-2000. *Ecology* 72:1896-1900.
- Hill, R. 1924. A lens for whole sky photographs. *Quarterly Journal of the Royal Meteorological Society* 50:227-235.
- Landry, R., R.A. Fournier, R. Lang, and F.J. Ahern. 1997. Tree vectorization: A method to describe tree architecture. *Canadian Journal of Remote Sensing* 23(2):91-107.
- Lang, A.R.G. 1986. Leaf area and average leaf angle from transmittance of direct sunlight. *Australian Journal of Botany* 34:349-355.



- Lang, A.R.G., R.E. McMurtrie, and M.L. Benson. 1991. Validity of surface area indices of *Pinus radiata* estimated from transmittance of the sun's beam. *Agricultural and Forest Meteorology* 37:229-243.
- Lerdau, M.T., N.M. Holbrook, H.A. Mooney, P.M. Rich, and J.L. Whitbeck. 1992. Seasonal patterns of acid fluctuations and resource storage in the arborescent cactus *Opuntia excelsa* in relation to light availability and size. *Oecologia* 92:166-171.
- Lin, T., P.M. Rich, D.A. Heisler, and F.J. Barnes. 1992. Influences of canopy geometry on near-ground solar radiation and water balances of pinyon-juniper and ponderosa pine woodlands. *American Society for Photogrammetry and Remote Sensing Technical Papers*, pp. 285-294.
- Miller, J.B. 1967. A formula for average foliage density. *Australian Journal of Botany* 15:141-144.
- Mitchell, P.L. and T.C. Whitmore. 1993. Use of hemispherical photographs in forest ecology: Calculation of absolute amount of radiation beneath the canopy. Oxford Forestry Institute, Oxford, United Kingdom.
- Neumann, H.H. and R.H. Shaw. 1989. Leaf area measurements based on hemispheric photographs and leaf-litter collection in a deciduous forest during autumn leaf-fall. *Agricultural and Forest Meteorology* 45:325-345.
- Newcomer, J., D. Landis, S. Conrad, S. Curd, K. Huemmerich, D. Knapp, A. Morrell, J. Nickeson, A. Papagno, D. Rinker, R. Strub, T. Twine, F. Hall, and P. Sellers, eds. 2000. Collected Data of The Boreal Ecosystem-Atmosphere Study. NASA. CD-ROM.
- Norman, J.M. and G.S. Campbell. 1989. Canopy structure. In *Plant Physiological Ecology: Field Methods and Instrumentation*. R.W. Pearcy, J. Ehleringer, H.A. Mooney, and P.W. Rundel (eds.). Chapman and Hall, New York, pp.301-326.
- Pearcy, R.W. 1989. Radiation and light measurements. In: R.W. Pearcy, J. Ehleringer, H.A. Mooney, and P.W. Rundel (eds.), *Plant Physiological Ecology: Field Methods and Instrumentation*. Chapman and Hall, New York, pp.95-116.
- Reifsnyder, W.E. 1967. Radiation geometry in the measurement and interpretation of radiation balance. *Agricultural and Forest Meteorology* 4:255-265.
- Rich, P.M. 1988. Video image analysis of hemispherical canopy photography. In: *First Special Workshop on Videography*. P.W. Mausel (ed.). American Society for Photogrammetry and Remote Sensing, Terre Haute, Indiana, May 19-20, 1988, pp. 84-95.
- Rich, P.M. 1989. A manual for analysis of hemispherical canopy photography. Los Alamos National Laboratory Report LA-11733-M.
- Rich, P.M. 1990. Characterizing plant canopies with hemispherical photographs. In: *Instrumentation for studying vegetation canopies for remote sensing in optical and thermal infrared regions*, N.S. Goel and J.M. Norman (eds.). *Remote Sensing Reviews* 5:13-29.
- Rich, P.M., D.A. Clark, D.B. Clark, and S.F. Oberbauer. 1993. Long-term study of solar radiation regimes in a tropical wet forest using quantum sensors and hemispherical photography. *Agricultural and Forest Meteorology* 65:107-127.
- Rich, P.M., J. Chen, S.J. Sulatycki, R. Vashisht, and W.S. Wachspress. 1995. Calculation of leaf area index and other canopy indices from gap fraction: a manual for the LAICalc software. Kansas Applied Remote Sensing Program Open File Report. Lawrence, KS.

Sellers, P. and F. Hall. 1994. Boreal Ecosystem-Atmosphere Study: Experiment Plan. Version 1994-3.0, NASA BOREAS Report (EXPLAN 94).

Sellers, P. and F. Hall. 1996. Boreal Ecosystem-Atmosphere Study: Experiment Plan. Version 1996-2.0, NASA BOREAS Report (EXPLAN 96).

Sellers, P., F. Hall, and K.F. Huemmrich. 1996. Boreal Ecosystem-Atmosphere Study: 1994 Operations. NASA BOREAS Report (OPS DOC 94).

Sellers, P., F. Hall, and K.F. Huemmrich. 1997. Boreal Ecosystem-Atmosphere Study: 1996 Operations. NASA BOREAS Report (OPS DOC 96).

Sellers, P., F. Hall, H. Margolis, B. Kelly, D. Baldocchi, G. den Hartog, J. Cihlar, M.G. Ryan, B. Goodison, P. Crill, K.J. Ranson, D. Lettenmaier, and D.E. Wickland. 1995. The boreal ecosystem-atmosphere study (BOREAS): an overview and early results from the 1994 field year. *Bulletin of the American Meteorological Society*. 76(9):1549-1577.

Sellers, P.J., F.G. Hall, R.D. Kelly, A. Black, D. Baldocchi, J. Berry, M. Ryan, K.J. Ranson, P.M. Crill, D.P. Lettenmaier, H. Margolis, J. Cihlar, J. Newcomer, D. Fitzjarrald, P.G. Jarvis, S.T. Gower, D. Halliwell, D. Williams, B. Goodison, D.E. Wickland, and F.E. Guertin. 1997. BOREAS in 1997: Experiment Overview, Scientific Results and Future Directions. *Journal of Geophysical Research* 102(D24): 28,731-28,770.

Turner, I.M. 1990. Tree seedling growth and survival in a Malaysian rain forest. *Biotropica*, 22:146-154.

Turton, S.M. 1988. Solar radiation regimes in a north Queensland rainforest. *Proceedings of the Ecological Society of Australia*, 15:101-105.

Weiss, S.B., P.M. Rich, D.D. Murphy, W.H. Calvert, and P.R. Ehrlich. 1991. Forest canopy structure at overwintering monarch butterfly sites: measurements with hemispherical photography. *Conservation Biology* 5:165-175.

Welles, J.M. 1990. Some indirect methods of estimating canopy structure. *Remote Sensing Reviews* 5:31-43.

### **17.3 Archive/DBMS Usage Documentation**

None.

## **18. Glossary of Terms**

None.

## 19. List of Acronyms

ASCII	- American Standard Code for Information Interchange
BOREAS	- BOReal Ecosystem-Atmosphere Study
BORIS	- BOREAS Information System
CCD	- Charge-Coupled Device
CCRS	- Canada Centre for Remote Sensing
CD-ROM	- Compact Disk-Read-Only Memory
DAAC	- Distributed Active Archive Center
DSF	- Direct Site Factor
EOS	- Earth Observing System
EOSDIS	- EOS Data and Information System
FIPAR	- Fraction of Intercepted PAR
GEMLAB	- GIS and Environmental Modeling Laboratory
GIS	- Geographic Information System
GSFC	- Goddard Space Flight Center
HTML	- HyperText Markup Language
IFC	- Intensive Field Campaign
ISF	- Indirect Site Factor
KU	- University of Kansas
LAI	- Leaf Area Index
MIX	- Mixed Wood
NAD83	- North American Datum of 1983
NASA	- National Aeronautics and Space Administration
NOAA	- National Oceanic and Atmospheric Administration
NSA	- Northern Study Area
OA	- Old Aspen
OBS	- Old Black Spruce
OJP	- Old Jack Pine
ORNL	- Oak Ridge National Laboratory
PANP	- Prince Albert National Park
PAR	- Photosynthetically Active Radiation
RSS	- Remote Sensing Science
SSA	- Southern Study Area
TE	- Terrestrial Ecology
TF	- Tower Flux
URL	- Uniform Resource Locator
UTM	- Universal Transverse Mercator
YA	- Young Aspen
YBS	- Young Black Spruce
YJP	- Young Jack Pine

## 20. Document Information

### 20.1 Document Revision Date

Written: 05-Mar-1997

Updated: 08-Oct-1999

### 20.2 Document Review Date(s)

BORIS Review: 04-May-1999

Science Review: 09-Dec-1998

## **20.3 Document ID**

## **20.4 Citation**

When using these data, please include the following acknowledgment as well as citations of relevant papers in Section 17.2:

The hemispherical photography data were collected for BOREAS by science team TE-23 under the direction of P.M. Rich at the University of Kansas.

Acknowledgments -- People:

The hemispherical photograph data set was collected and analyzed for BOREAS under the direction of P.M. Rich at the University of Kansas. The dedicated efforts of Y.R. Alger and V.L. Peterson are acknowledged in collecting and preparing these data. P. Albu, D. Archer, C. Poschadel, D. Miller, W. Smith, and J. Vogel assisted with data acquisition, J. Chen of the Canada Centre for Remote Sensing collaborated in calculations, M. Apps of Forestry Canada provided logistical assistance and accommodations, and R.A. Fournier and N.M. August of the Canada Centre for Remote Sensing provided scientific input and field assistance.

Acknowledgments -- Organizations/Funding Sources:

This work was supported by the Canada Centre for Remote Sensing, Forestry Canada, the Kansas Applied Remote Sensing Program, the Kansas Biological Survey, the Kansas Center for Computer Aided Systems Engineering, NASA grant NAG5-2358, and the University of Kansas Research Development and General Research Funds.

If using data from the BOREAS CD-ROM series, also reference the data as:

Rich, P.M., "Canopy Architecture of Boreal Forests: Using Hemispherical Photography for Study of Radiative Transport and Leaf Area Index." In *Collected Data of The Boreal Ecosystem-Atmosphere Study*. Eds. J. Newcomer, D. Landis, S. Conrad, S. Curd, K. Huemmrich, D. Knapp, A. Morrell, J. Nickeson, A. Papagno, D. Rinker, R. Strub, T. Twine, F. Hall, and P. Sellers. CD-ROM. NASA, 2000.

Also, cite the BOREAS CD-ROM set as:

Newcomer, J., D. Landis, S. Conrad, S. Curd, K. Huemmrich, D. Knapp, A. Morrell, J. Nickeson, A. Papagno, D. Rinker, R. Strub, T. Twine, F. Hall, and P. Sellers, eds. *Collected Data of The Boreal Ecosystem-Atmosphere Study*. NASA. CD-ROM. NASA, 2000.

## **20.5 Document Curator**

## **20.6 Document URL**

# REPORT DOCUMENTATION PAGE

*Form Approved*  
OMB No. 0704-0188

Public reporting burden for this collection of information is estimated to average 1 hour per response, including the time for reviewing instructions, searching existing data sources, gathering and maintaining the data needed, and completing and reviewing the collection of information. Send comments regarding this burden estimate or any other aspect of this collection of information, including suggestions for reducing this burden, to Washington Headquarters Services, Directorate for Information Operations and Reports, 1215 Jefferson Davis Highway, Suite 1204, Arlington, VA 22202-4302, and to the Office of Management and Budget, Paperwork Reduction Project (0704-0188), Washington, DC 20503.

<b>1. AGENCY USE ONLY</b> ( <i>Leave blank</i> )		<b>2. REPORT DATE</b> October 2000	<b>3. REPORT TYPE AND DATES COVERED</b> Technical Memorandum	
<b>4. TITLE AND SUBTITLE</b> Technical Report Series on the Boreal Ecosystem-Atmosphere Study (BOREAS) BOREAS TE-23 Canopy Architecture and Spectral Data from Hemispherical Photographs			<b>5. FUNDING NUMBERS</b>  923 RTOP: 923-462-33-01	
<b>6. AUTHOR(S)</b> Paul M. Rich Forrest G. Hall and Andrea Papagno, Editors				
<b>7. PERFORMING ORGANIZATION NAME(S) AND ADDRESS (ES)</b>  Goddard Space Flight Center Greenbelt, Maryland 20771			<b>8. PERFORMING ORGANIZATION REPORT NUMBER</b>  2000-03136-0	
<b>9. SPONSORING / MONITORING AGENCY NAME(S) AND ADDRESS (ES)</b>  National Aeronautics and Space Administration Washington, DC 20546-0001			<b>10. SPONSORING / MONITORING AGENCY REPORT NUMBER</b>  TM—2000—209891 Vol. 187	
<b>11. SUPPLEMENTARY NOTES</b> P.M. Rich: University of Kansas, Lawrence; A. Papagno: Raytheon ITSS, NASA Goddard Space Flight Center, Greenbelt, Maryland				
<b>12a. DISTRIBUTION / AVAILABILITY STATEMENT</b> Unclassified—Unlimited Subject Category: 43 Report available from the NASA Center for AeroSpace Information, 7121 Standard Drive, Hanover, MD 21076-1320. (301) 621-0390.			<b>12b. DISTRIBUTION CODE</b>	
<b>13. ABSTRACT</b> ( <i>Maximum 200 words</i> )  The BOREAS TE-23 team collected hemispherical photographs in support of its efforts to characterize and interpret information on estimates of canopy architecture and radiative transfer properties for most BOREAS study sites. Various OA, OBS, OJP, YJP, and YA sites in the boreal forest were measured from May to August 1994. The hemispherical photographs were used to derive values of LAI, leaf angle, gap fraction, and clumping index. This documentation describes these derived values. The derived data are stored in tabular ASCII files. The hemispherical photographs are stored in the original set of 42 CD-ROMs that were supplied by TE-23.				
<b>14. SUBJECT TERMS</b> BOREAS, terrestrial ecology, canopy architecture, radiative transfer properties.			<b>15. NUMBER OF PAGES</b> 48	
			<b>16. PRICE CODE</b>	
<b>17. SECURITY CLASSIFICATION OF REPORT</b> Unclassified	<b>18. SECURITY CLASSIFICATION OF THIS PAGE</b> Unclassified	<b>19. SECURITY CLASSIFICATION OF ABSTRACT</b> Unclassified	<b>20. LIMITATION OF ABSTRACT</b> UL	

